Article

Current Biology

Receptor-like-kinase-interacting protein TOW stabilizes PIN transporters for auxin canalization

Highlights

- TOW is an auxin-inducible gene downstream of TIR1/AFB and WRKY23
- TOW is required for auxin canalization and vascular regeneration
- TOW interacts with RLKs, including CAMEL-CANAR and TMK1/4
- TOW stabilizes PIN1 at the membrane to promote canalization

Authors

Mingyue Li, Nikola Rydza, Ewa Mazur, Gergely Molnár, Tomasz Nodzyński, Jiří Friml

Correspondence

jiri.friml@ist.ac.at

In brief

Li et al. identify a novel plant protein, TOW, whose expression is induced by the phytohormone auxin. TOW promotes the interaction of PIN auxin transporters with canalization-related receptor-like kinases and stabilizes PINs at the plasma membrane. This enables auxin canalization-related processes such as vein patterning and vascular regeneration.

Li et al., 2026, Current Biology *36*, 1468–1480
March 23, 2026
https://doi.org/10.1016/j.cub.2026.02.023

CellPress

CellPress
OPEN ACCESS

Current Biology

Article

Receptor-like-kinase-interacting protein TOW stabilizes PIN transporters for auxin canalization

Mingyue Li,[1] Nikola Rydza,[2] Ewa Mazur,[3] Gergely Molnár,[1] Tomasz Nodzyński,[2] and Jiří Friml[1,4,*]
[1]Institute of Science and Technology Austria (ISTA), 3400 Klosterneuburg, Austria
[2]Mendel Centre for Plant Genomics and Proteomics, Central European Institute of Technology (CEITEC), Masaryk University, Kamenice 5, 625 00 Brno, Czechia
[3]Institute of Biology, Biotechnology and Environmental Protection, Faculty of Natural Sciences, University of Silesia in Katowice, Katowice, Poland
[4]Lead contact
*Correspondence: jiri.friml@ist.ac.at
https://doi.org/10.1016/j.cub.2026.02.023

SUMMARY

Auxin canalization is a self-organizing process that governs the flexible formation of vasculature by reinforcing the formation of auxin transport channels. A key prerequisite is the feedback between auxin signaling and directional auxin transport, mediated by PIN transporters. Despite the developmental importance of canalization, the molecular components linking auxin perception to the regulation of PIN auxin transporters remain poorly understood. Here, we identify TOW, a novel and essential component of auxin canalization that links intracellular auxin signaling with cell surface auxin perception. TOW is regulated downstream of TIR1/AFB-Aux/IAA-WRKY23 transcriptional auxin signaling. *tow* mutants exhibit defects in regeneration and *de novo* vasculature formation, along with impaired formation of polarized, PIN-expressing auxin channels. At the subcellular level, these mutants display disrupted auxin-induced PIN polarization and altered PIN endocytic trafficking dynamics. TOW localizes predominantly to the plasma membrane, where it interacts with receptor-like kinases involved in auxin canalization, including the TMK1 auxin co-receptor and the CAMEL-CANAR complex. TOW promotes PIN interaction with these kinases and stabilizes PINs at the cell surface. Together, our findings identify TOW as a molecular link between intracellular and cell surface auxin signaling mechanisms that converge on PIN trafficking and polarity, providing new insights into how auxin signaling regulates directional auxin transport for the self-organizing formation of vasculature during flexible plant development.

INTRODUCTION

Plants have evolved delicate mechanisms to adapt their architecture to environmental conditions. Much of this adaptive development is achieved through the self-organization of patterning processes, including the integration of new organs into the pre-existing vascular network, the emergence of complex leaf venation patterns, and the flexible regeneration of vasculature around wounds. Previous studies have identified auxin as the primary phytohormone involved in these processes, in particular, in the spontaneous formation and differentiation of vascular strands in different contexts.[1] The auxin canalization hypothesis was proposed, suggesting that the directional movement of an auxin-dependent signal through a field of cells enhances the ability of individual cells to transport auxin. This positive feedback mechanism linking auxin and its transport leads to the gradual formation of narrow auxin transport channels.[2] While the canalization hypothesis is both mechanistically fascinating and developmentally crucial—and is well supported by mathematical modeling[2,3]—the underlying genetic basis remains largely unknown.

Polarly localized PIN auxin efflux transporters are key components that facilitate directional cell-to-cell auxin flow in plants.[4] PIN polarity, which is a key determinant of auxin flow directionality,[5] is extensively regulated by phosphorylation and depends on endosomal trafficking,[6,7] and both processes are targeted by many endogenous and environmental signals.[4] It has been repeatedly demonstrated that PIN polarity can be dynamically rearranged also by auxin.[5,8,9] Auxin treatment promotes the relocation of PIN proteins from the basal to the lateral side of root cells in a tissue-specific manner. Intriguingly, mutants with defects in this auxin-induced PIN lateralization exhibit typically abnormal leaf venation and vasculature formation,[10–12] reinforcing the idea that auxin feedback on PIN polarity is essential for vascular patterning, as proposed by the auxin canalization hypothesis. Yet the molecular players coordinating PIN polarity, auxin transport, and endosomal trafficking during canalization remain largely unknown.

The canonical auxin signaling mechanism has been well characterized, involving the TIR1/AFB (TRANSPORT INHIBITOR RESPONSE 1/AUXIN-SIGNALING F-BOX), Aux/IAA (AUXIN/INDOLE-3-ACETIC ACID), and ARF (AUXIN RESPONSE FACTOR) components.[13] Mutants with defects in auxin signaling typically display disrupted vascular strand formation and abnormal leaf vein patterns.[5,8,14] Transcriptional profiling of SCF^{TIR1}-Aux/IAA-ARF signaling identified WRKY DNA-BINDING

PROTEIN 23 (WRKY23) as a downstream regulator required for PIN lateralization and auxin canalization.[8] These findings suggest that the SCF^{TIR1}-Aux/IAA-WRKY23 signaling pathway is essential for auxin-mediated PIN polarity regulation during canalization. However, WRKY23 as a transcriptional regulator is not directly involved in trafficking or polarization processes, raising the problem of identifying direct molecular players that mediate coordinated PIN polarity rearrangements during auxin canalization and beyond.

Among the downstream components of SCF^{TIR1}-Aux/IAA-WRKY23 involved in PIN polarity regulation, the leucine-rich repeat receptor-like kinase (LRR-RLK), named CANALIZATION-RELATED AUXIN-REGULATED MALECTIN-TYPE RLK (CAMEL), has been identified.[12] Together with its interactor, CANALIZATION-RELATED RLK (CANAR), CAMEL phosphorylates PIN proteins, leading to their repolarization.

Notably, besides intracellular TIR1/AFB-mediated auxin signaling, also cell surface auxin perception mediated by AUXIN-BINDING PROTEIN1 (ABP1) and its LRR-RLK interactors TRANSMEMBRANE KINASEs (TMKs) is essential for auxin canalization-mediated processes such as *de novo* vasculature formation and regeneration.[15] The ABP1-TMK signaling-dependent regulation of auxin transport may occur via direct interaction of TMKs with PIN auxin transporters and their subsequent phosphorylation.[16,17] Nonetheless, how ABP1-TMK and TIR1/AFB auxin perception mechanisms are integrated with each other and with CAMEL-CANAR-mediated canalization mechanisms remains unclear.

In this study, we identified target of WRKY23 (TOW), a previously uncharacterized membrane protein essential for auxin canalization, PIN polarity, and trafficking. TOW is a downstream effector of the SCF^{TIR1}-Aux/IAA-WRKY23 signaling and interacts with both ABP1-TMK1 and CAMEL/CANAR signaling modules. Collectively, our findings establish TOW as a pivotal integrator of intracellular and cell surface auxin signaling with RLK-mediated PIN trafficking and polarity control, which is essential for executing auxin canalization during vascular development.

RESULTS

TOW is a downstream target of SCF^{TIR1}-Aux/IAA-WRKY23 signaling

To identify additional molecular factors involved in auxin canalization-dependent, self-organizing vasculature formation downstream of SCF^{TIR1}-Aux/IAA-WRKY23, we analyzed transcriptomics data of auxin-responsive genes,[18] Aux/IAA-dependent genes,[8] and WRKY23-dependent genes[12] from previously published studies. The overlap between the auxin-responsive dataset and the Aux/IAA-induced gene set revealed a group of 245 genes that are auxin-induced and dependent on SCF^{TIR1}-Aux/IAA-ARF signaling. Further comparison with WRKY23-dependent microarray data led to a final list of 53 genes as potential targets of the SCF^{TIR1}-Aux/IAA-WRKY23 signaling (Figure S1A). This group includes the AGCIII kinase *PINOID* (*PID*),[19] a well-known regulator of PIN polarity,[20] along with numerous well-known components of transcriptional auxin signaling, including *AuxIAAs*, *ARFs*,[18] and various auxin-responsive genes such as SAURs, *LBD*s, and auxin biosynthetic enzymes like *GH3.1*, *GH3.3*, and *DFL1*. After filtering out these known components, we identified the uncharacterized gene *AT3G09280* as a potential novel factor required for auxin canalization (Figure S1A). We named this gene *TOW*.

RT-qPCR confirmed that *TOW* transcription is significantly upregulated by IAA in a time- and dose-dependent manner, showing an even faster and more sensitive response than *WRKY23* (Figures S1B and S1C). This upregulation is largely compromised in the *arf7 arf19* double mutant, confirming that TOW is a downstream target of SCF^{TIR1}-Aux/IAA-ARF signaling (Figure 1A). TOW transcription is also increased when the WRKY23 is conditionally activated in the dexamethasone (DEX)-inducible line (Figure 1B).

Consistent with the induction of TOW transcription by both ARFs and WRKY23, three auxin-responsive elements (AuxREs) and three W-box binding motifs are annotated in the TOW promoter region, according to the JASPAR database[21] (Figure S1D). Moreover, transactivation of the *TOW* promoter (using the *pTOW::DUAL-LUC* construct) by ARF7, ARF19, and WRKY23 after treatment with 1 μM IAA in *Nicotiana benthamiana* leaves (Figure 1C) further confirmed that TOW transcription can be activated by both ARF and WRKY23 transcription factors.

Overall, these results identify *TOW* as an auxin-responsive gene targeted by both SCF^{TIR1}-Aux/IAA-ARF and WRKY23 signaling.

TOW encodes a small transmembrane protein expressed in developing vasculature

Phylogenetic analysis based on the TOW amino acid sequence revealed that TOW is a plant-specific protein present exclusively in angiosperms (Figure S1E). In *Arabidopsis thaliana*, it is encoded by a single-copy gene. The most ancient identifiable ortholog is found in *Amborella trichopoda*, the earliest-diverging extant lineage of flowering plants (Figure S1E). The restriction of TOW to flowering plants suggests its involvement in processes specific to angiosperm development and physiology, possibly reflecting an evolutionary innovation linked to the emergence of complex vascular tissues or specialized auxin transport mechanisms.

Analysis of the TOW amino acid sequence revealed a predicted signal peptide at the N terminus and a putative transmembrane domain near the C terminus (Figure 1D). Evolutionary rate analysis showed high conservation scores within the transmembrane domain (Figure 1E), suggesting its functional importance. To investigate subcellular localization, we generated transgenic Arabidopsis plants expressing a *pTOW::TOW-GFP* construct. TOW-GFP predominantly localized to the plasma membrane (PM) in root epidermal and columella cells (Figure 1N), supporting its identity as a transmembrane protein.

To examine TOW expression patterns, we generated transgenic lines expressing a *GUS* (*β-glucuronidase*) reporter driven by a 2 kb *TOW* promoter. GUS staining revealed *TOW* expression in multiple tissues, including the primary root (Figure 1F), lateral root primordia (Figure 1H), lateral root cap (Figure 1I), shoot apical meristem (Figure 1J), inflorescence, and pollinated flowers (Figure 1K). Notably, TOW was also expressed in cotyledon leaf veins and at the cotyledon apex (Figure 1G), regions that coincide with known auxin accumulation maxima.[22] This spatial correlation suggests that TOW expression is responsive to endogenous auxin levels. Indeed, exogenous IAA application

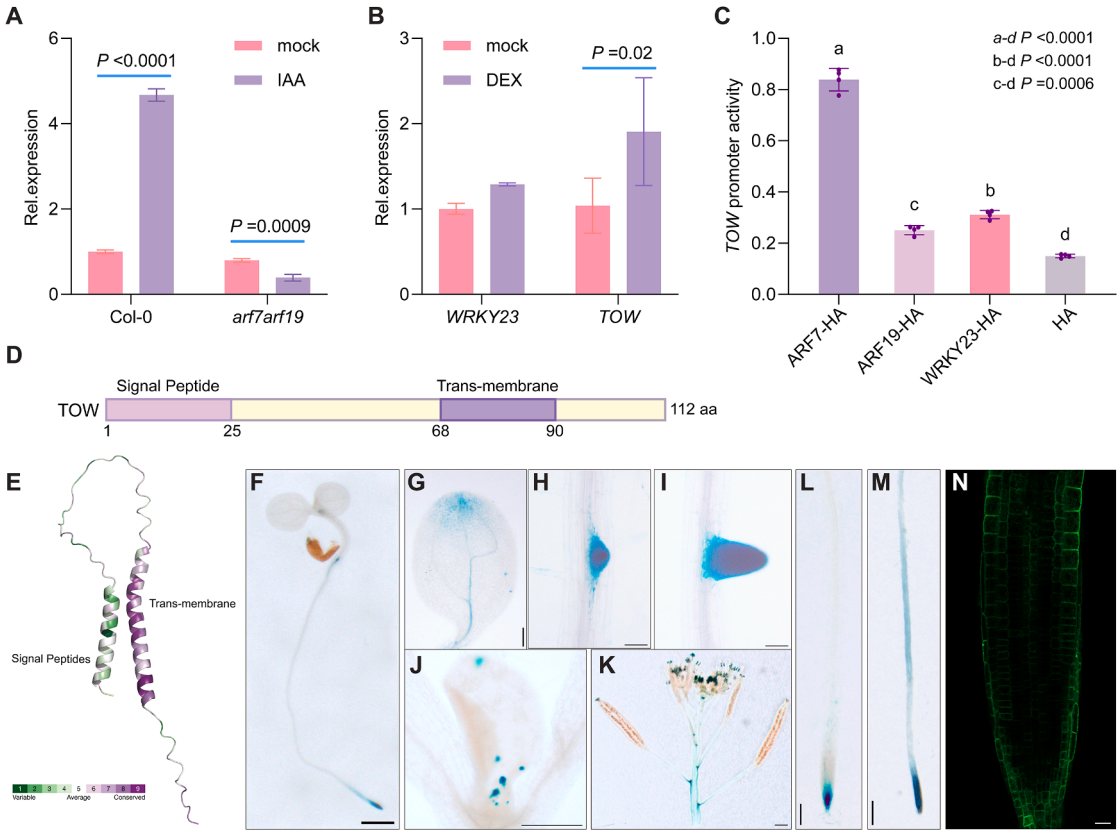

Figure 1. Membrane protein TOW is transcriptionally regulated by ARF and WRKY23 auxin signaling

(A and B) RT-qPCR analysis showing IAA-induced, ARF-dependent (A) as well as WRKY23-dependent (B) regulation of *TOW* transcription. For all RT-qPCR experiments, gene expression levels were normalized to *PP2A*. *p* values were calculated using two-way ANOVA followed by Tukey's post hoc test. Data are representative of three biological replicates and presented as mean ± SD.

(C) Transactivation of *pTOW::DUAL-LUC* by ARF or WRKY23 after treatment with 1 μM IAA for 24 h in co-transfected *Nicotiana benthaminana* leaves. Data are mean ± SD, $n = 3$ independent biological replicates. *p* values were determined using one-way ANOVA with Tukey's post hoc test.

(D) Predicted domain structure of the TOW protein.

(E) Evolutionary conservation scores of individual amino acids projected onto the predicted 3D structure of TOW.

(F–M) Histochemical visualization of GUS activity (blue) in *pTOW::GUS* reporter lines. 5-day-old seedling stained with GUS substrate in whole seedling (F), cotyledon (G), lateral root primordia (H), lateral root cap (I), shoot meristem (J), inflorescence with flowers (K), primary root before treatment (L), and after IAA treatment for 6 h (M).

(N) Subcellular localization of *pTOW::TOW-GFP* in the primary root tip ($n = 10$).

Scale bars, 1 mm (F, J, and K), 100 μm (G–I, L, and M), and 10 μm (N).

See also Figure S1.

significantly enhanced *TOW* expression in primary roots (Figures 1L and 1M), confirming the auxin-responsiveness of *TOW* expression. This expression pattern overlaps with and partially precedes the formation of differentiating vascular strands and coincides with PIN1-expressing vascular tissues, consistent with a role for TOW in auxin-induced, PIN1-mediated vascular development.

TOW mediates leaf venation and the underlying PIN1 polarized channel formation

Auxin canalization underlies several developmental processes, including leaf vein formation,[22] vascular regeneration after wounding,[10] and apical dominance.[23] To investigate whether TOW is required for these processes, we examined the leaf venation pattern in cotyledons of Col-0 and *tow* mutants. Four independent *tow* alleles were generated using the CRISPR-Cas9 system (Figure S2A). Among them, *tow-C1* and *tow-C3* carry in-frame deletions, while *tow-C2* and *tow-C4* harbor frameshift mutations that result in premature stop codons (Figure S2A).

While the majority of cotyledons in Col-0 displayed regular, four-loop venation, approximately 20.6% showed mild irregularities (Figures 2A and 2B). By contrast, *tow* mutants exhibited a significant increase in defective vein patterns, with 34.3%–40.7% of cotyledons affected. Notably, *tow-C1* and *tow-C3* displayed reduced vein loop numbers (21.2% and 16.7% of cotyledons), whereas *tow-C2* and *tow-C4* showed a higher frequency of disconnected bottom loops (*tow-C2*, 20.1%; *tow-C4*, 13.3%) (Figures 2B and S2B). These defects were largely rescued by introducing a *pTOW::TOW-GFP* construct into the *tow* background, restoring regular venation in 76.8% of

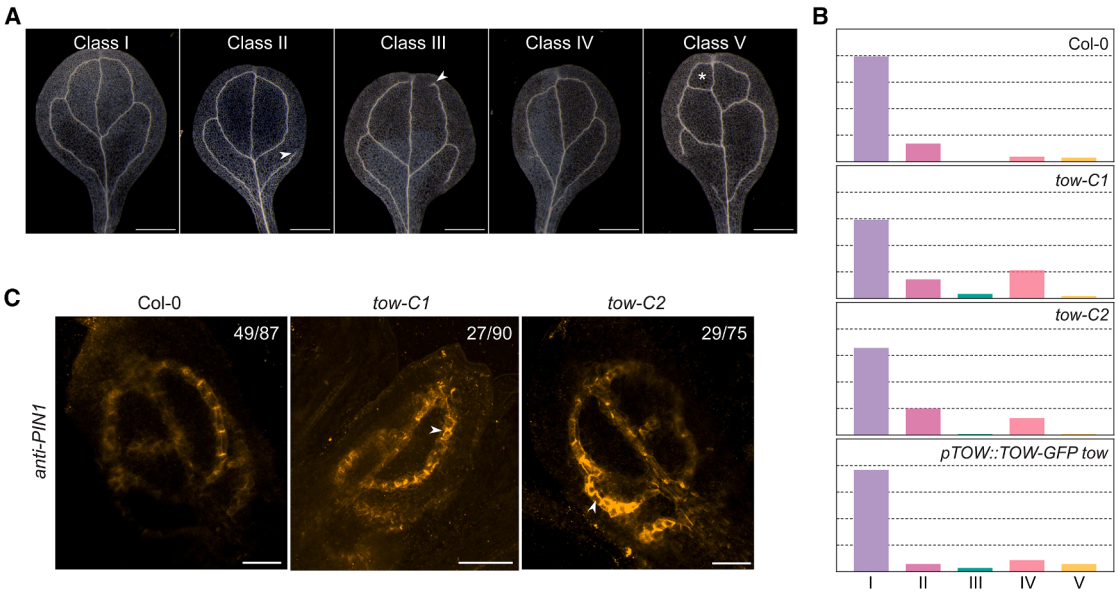

Figure 2. Abnormal patterning and PIN1 polarization during leaf venation in *tow* mutants

(A) Dark-field illumination of cleared cotyledons illustrating different venation patterning classes: normal venation pattern (class I), disconnected bottom loop (class II), disconnected upper loop (class III), fewer loops (class IV), and extra loops (class V). Scale bar, 1 mm.

(B) Percentage distribution of each venation patterning class in Col-0, *tow* mutants, and the complementation line. Dashed lines indicate 20%, 40%, 60%, and 80% thresholds. For each genotype, $n > 120$.

(C) Representative images showing PIN1 immunolocalization in the first leaves. The numbers in the top-left corners represent the incidence of observed PIN1 polarity localization relative to the number of leaves analyzed. White arrowheads indicate PIN1 polarity defects. Scale bar, 100 μm.

See also Figure S2.

cotyledons—comparable to Col-0 levels (Figure 2B). These results show that the TOW function is essential for proper leaf vein formation.

We used this phenotype to test the relationship between *WRKY23* and *TOW* genetically and generated *wrky23 tow* double mutants. Analysis of leaf venation patterns in *wrky23* and *wrky23 tow* mutants revealed no additive or synergistic phenotypes (Figure S2C), consistent with both regulators acting within the same pathway.

Polar auxin transport, mediated by PIN proteins, is the key prerequisite of the canalization mechanism.[5] Among the PIN family, PIN1 is the most informative marker for vein patterning, with its expression known to precede and predict vascular strand formation in developing leaves.[22] To determine whether the venation defects in *tow* mutants are associated with altered PIN1 localization, we performed immunolocalization in the first true leaves of Col-0 and *tow* mutants. In Col-0, PIN1 protein was directionally localized toward the leaf tip in early-stage secondary veins connecting to the midvein (49/87 observed) (Figure 2C). By contrast, *tow-C1* and *tow-C2* showed disrupted PIN1 polarity, with significantly fewer cells exhibiting tip-ward localization (27/90 in *tow-C1*, 29/75 in *tow-C2*). Instead, PIN1 signals were often misoriented toward lateral sides—either inward toward the midvein or outward toward the leaf margin (Figure 2C). This loss of coherent PIN1 polarity likely impairs auxin flux and compromises the establishment of continuous vascular strands.

Together, these findings identify a role for TOW in mediating the PIN1 polarization in forming vasculature during leaf vein formation.

TOW mediates vasculature regeneration and auxin canalization

Next, we assessed vascular regeneration in *tow* mutants. When a transverse incision was introduced into the inflorescence stem, 90% of Col-0 plants (n = 10) were able to regenerate new vascular strands around the wound site, as visualized by the toluidine blue (TBO) staining (Figures 3A and 3B). By contrast, complete vascular reconnection occurred in only 10% of *tow-C1* (n = 10) and 20% of *tow-C2* (n = 10) mutants. Notably, 50% of *tow-C1* and 40% of *tow-C2* failed to regenerate vasculature entirely, while the remaining 40% in both lines formed only partial new vessel cells (Figure 3B).

To directly assess auxin canalization potential, we performed an auxin-induced vascular formation assay by excising the apical portion of the stem to remove endogenous auxin sources and applying an IAA droplet just below the wound.[14,23] In Col-0 (n = 10), new vasculature formed in 80% of treated stems, connecting the IAA application site with existing vascular bundles (Figure 3C). By contrast, *tow-C1* (n = 10) and *tow-C2* (n = 10) showed strong defects in this process, with only 20% and 30% forming continuous vascular strands, respectively. Approximately 40% of *tow-C1* and 30% of *tow-C2* showed completely abolished new vasculature formation, while the remaining 40% in both lines developed only partial connections (Figure 3D). To explore whether these defects correlate with the disrupted formation of auxin transport channels, we used the *pPIN1::PIN1-GFP* reporter line. In Col-0 (n = 10), polarized PIN1 expression formed a clear channel around the wound in about 70% of samples (Figures 3E and 3F). In *tow-C1* (n = 10), no completed PIN1

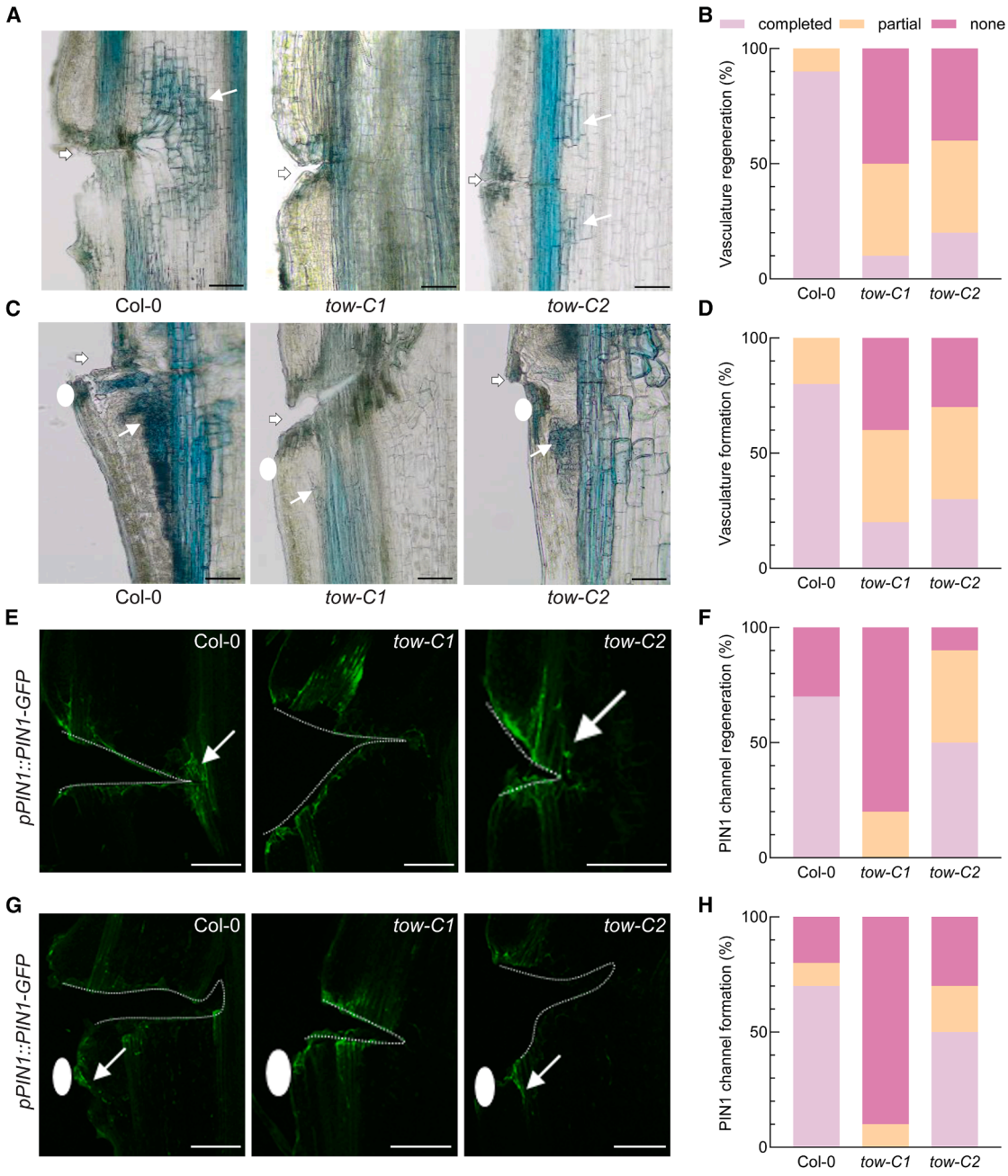

Figure 3. Defective vascular regeneration and auxin canalization in *tow* mutants

(A–D) Vascular regeneration (A) or auxin-induced vasculature formation (C) in wounded stems of Col-0 and *tow* mutants with its quantification (B and D). Vasculature is visualized by TBO staining. For each genotype, $n = 10$. The wound site is indicated by a white arrowhead, and newly regenerated vessel elements are marked with white arrows. The site of auxin application is marked by a white circle.

(E–H) Visualization of newly formed PIN1-GFP channels following stem wounding (E) or after local auxin application (G) in Col-0 and *tow* mutants with the quantification (F and H). $n = 10$ for each genotype. The wounding site is outlined with a dashed line, and regenerated PIN1-GFP channels are indicated by white arrows. The auxin application site is marked by a white circle. Scale bar, 100 μm.

See also Figure S3.

channel formation was detected. 80% of samples lacked any discernible channel, and 20% showed only partial formation. *tow-C2* mutants ($n = 10$) displayed intermediate defects, with 10% failing to form a channel and 40% forming partial channels (Figure 3F). Following local auxin application, 70% of Col-0 ($n = 10$) developed clear PIN1 channels (Figures 3G and 3H). By contrast, 90% of *tow-C1* samples ($n = 10$) failed to form any detectable channel, whereas *tow-C2* ($n = 10$) again showed

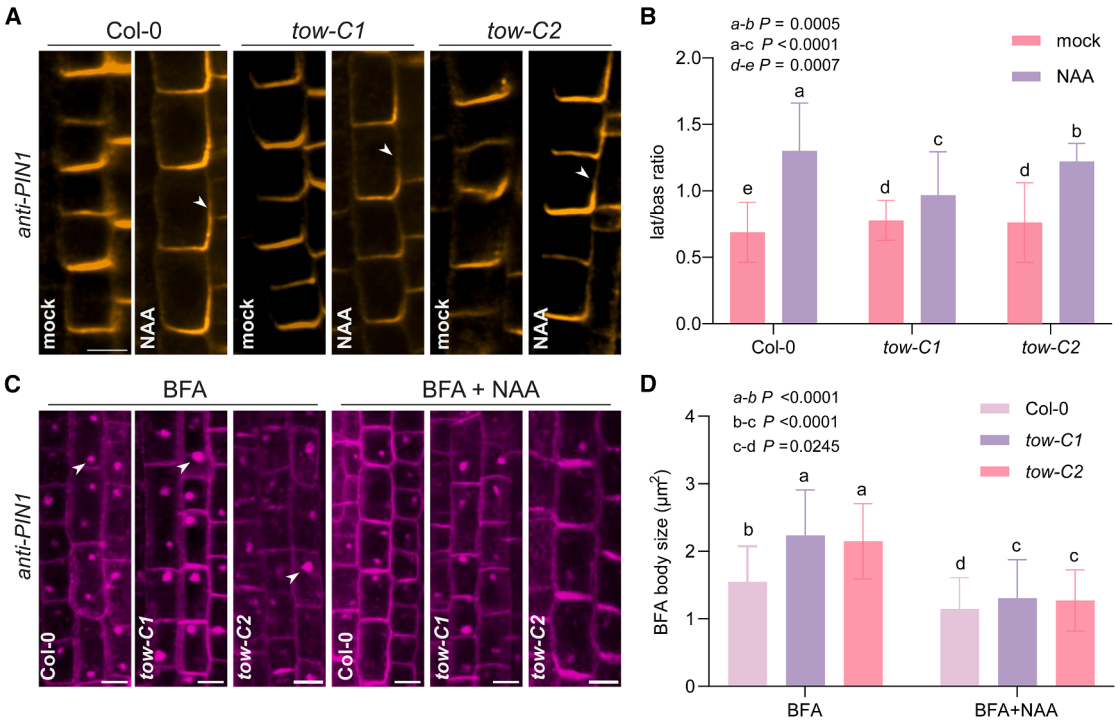

Figure 4. Defective PIN1 polarity and trafficking in *tow* mutants

(A and B) Immunolocalization of PIN1 in endodermal cells of the root meristem following treatment with 10 µM naphthaleneacetic acid (NAA) for 4 h. Arrowheads indicate lateral PIN1 signals. Scale bar, 10 µm. Quantification of lateral-to-basal PIN1 signal intensity (B).

(C and D) Representative confocal images of BFA bodies in root meristem cells after PIN1 immunostaining. Seedlings were treated with 50 µM brefeldin A (BFA) for 1 h or co-treated with 50 µM BFA and 10 µM NAA for 1 h. PIN1-labeled BFA bodies are indicated with arrowheads. Scale bar, 10 µm. Quantification of BFA body size (D) under BFA or BFA + NAA treatment.

For (B) and (D), data are presented as mean ± SD from three independent experiments, and one representative experiment is shown. Statistical significance was determined using two-way ANOVA followed by Tukey's post hoc test. Different letters indicate statistically significant differences, $p < 0.05$. $n > 200$ cells for each genotype.

See also Figure S4.

intermediate defects, with 30% lacking and 20% displaying partial channel formation (Figures 3G and 3H).

Notably, TOW expression was strongly induced upon wounding and local auxin application (Figures S3A and S3B), mirroring PIN1 expression patterns. These findings support a role for TOW in regulating the formation of directional PIN1-expressing channels during auxin canalization.

To elucidate the role of TOW in root development, we examined primary and lateral root development in *tow* mutant and complementation lines. The *tow-C1* and *tow-C2* mutants showed comparable primary root lengths to Col-0, although *tow-C2* exhibited slightly shorter roots (Figure S3C). Nonetheless, *tow-C2* displayed a significantly higher lateral root density relative to Col-0, which was fully rescued in the *pTOW::TOW-GFP tow* complementation line (Figure S3D). Moreover, both *tow-C1* and *tow-C2* exhibited significantly longer lateral roots compared with Col-0, which was also complemented by the *pTOW::TOW-GFP* construct (Figure S3E). On the other hand, root gravitropic responses were indistinguishable among *tow-C1, tow-C2, 35S::TOW-GFP*, and Col-0 seedlings (Figure S3F).

Together, our data demonstrate that TOW is essential for characterizing auxin canalization-associated processes, likely by facilitating the formation of polarized, PIN1-expressing channels required for subsequent vascular patterning.

TOW regulates PIN polarity and endocytic trafficking

To investigate whether TOW regulates PIN1 polarity, we first examined auxin-induced PIN repolarization in the root, a well-established hallmark of auxin canalization.[5] In Col-0 roots, treatment with synthetic auxin naphthaleneacetic acid (NAA) promotes the lateralization of basally localized PIN1 to the inner lateral sides of endodermal and pericycle cells.[5] This repolarization response was significantly impaired in both *tow-C1* ($n = 310$ cells) and *tow-C2* ($n = 305$ cells) mutants (Figures 4A and 4B). Similar defects were observed for PIN2 lateralization in cortex and epidermal cells (Figures S4E and S4G), indicating a general disruption of auxin-induced PIN repolarization in the absence of TOW. These defects were fully rescued in the *pTOW::TOW-GFP tow* complementation line (Figures S4A, S4B, S4E, and S4G), confirming that TOW is required for auxin regulation of PIN polarity.

Next, we examined whether TOW influences PIN trafficking. PIN proteins undergo constitutive endocytic recycling, and this can be monitored by treatment with brefeldin A (BFA), a fungal toxin that inhibits ARF-GEF-mediated vesicle budding. BFA

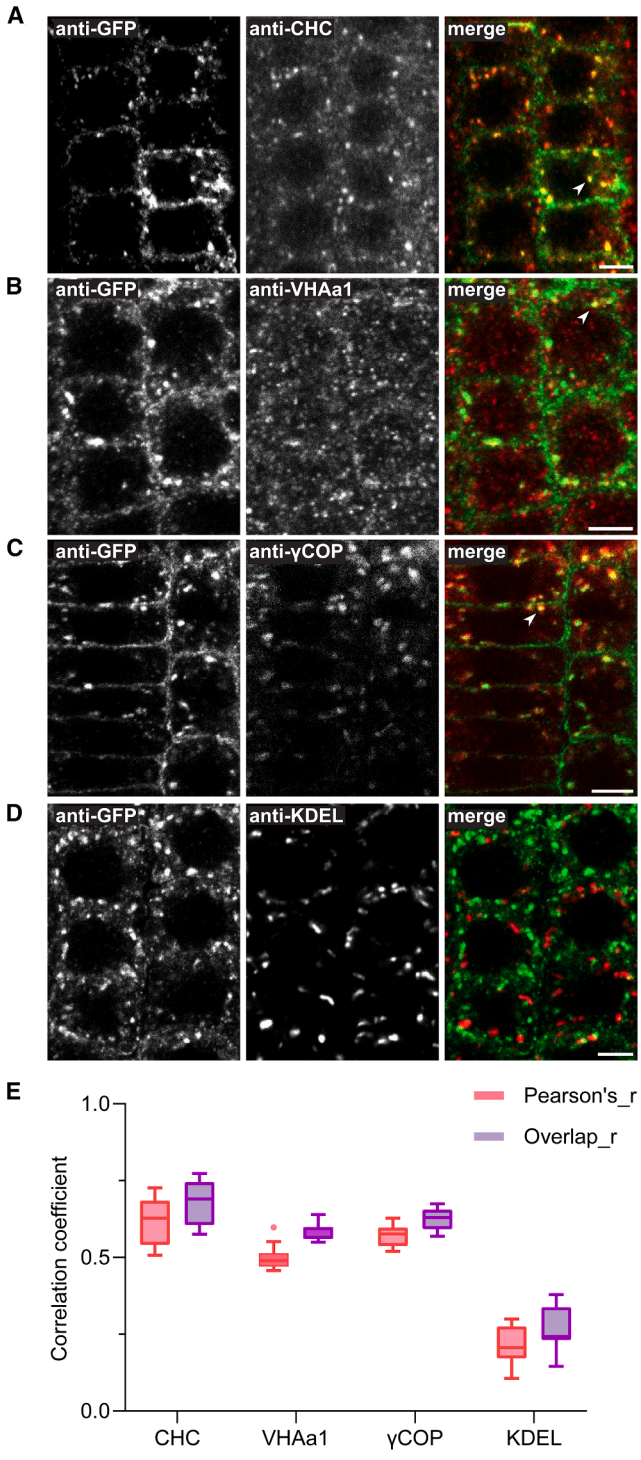

Figure 5. Subcellular localization of TOW at the PM, TGN, and Golgi

(A–D) Immunolocalization of GFP-tagged TOW in the *tow*-complementing line co-immunostained with subcellular markers: clathrin heavy chain (CHC) for the *trans*-Golgi network (TGN) (A), VHAa1 for TGN/early endosomes (TGN/EE) (B), γCOP for the Golgi apparatus (C), and KDEL-containing proteins for the endoplasmic reticulum (ER) (D). For each co-localization experiment, $n > 12$ roots. Scale bars, 5 μm.

(E) Quantification of co-localization between *pTOW::TOW-GFP* and each marker. Pearson's correlation coefficient (Pearson's_r) and the overlap coefficient (Overlap_r) were calculated from at least 12 roots per marker. Data are presented as a Tukey boxplot, where the box represents the interquartile range (25th to 75th percentile), the line inside the box indicates the median, and the whiskers extend to the extreme data points within 1.5 times the interquartile range. The individual dot represents outliers beyond this range.

treatment leads to the accumulation of PIN proteins into intracellular aggregates called BFA bodies.[24] By contrast, auxin inhibits PIN endocytosis and therefore reduces BFA body formation.[25] After treatment with 50 μM BFA for 1 h, PIN1- and PIN2-labeled BFA bodies were observed in Col-0 ($n = 236$ cells), *tow* mutants, and the complementary line. However, *tow-C1* ($n = 230$ cells) and *tow-C2* ($n = 230$ cells) mutants developed significantly larger BFA bodies than Col-0 (Figures 4C, 4D, S4F, and S4H), suggesting a defect in PIN trafficking. This phenotype was fully rescued in the *pTOW::TOW-GFP tow* complementation line (Figures S4C, S4D, S4F, and S4H), confirming the involvement of TOW in BFA-sensitive PIN trafficking.

Importantly, the excessive accumulation of PIN proteins in the BFA body was significantly reduced by exogenous NAA treatment in both Col-0 and *tow* mutants (Figures 4C and 4D), further highlighting that TOW is essential for integrating these antagonistic signals to maintain balanced PIN trafficking dynamics.

Together, these findings suggest that TOW is required for both auxin-induced PIN repolarization and for maintaining the PIN endocytic trafficking. The defects in *tow* mutants point to a role for TOW in a regulatory network that controls PIN polarity, potentially by modulating BFA-sensitive trafficking components or interacting with PIN polarity regulators such as kinases.

Subcellular localization of TOW at the Golgi, TGN, and PM

As previously mentioned, TOW predominantly localizes to the PM (Figure 1N). However, a portion of TOW was also detected in endomembranes within the cell interior. To further characterize the intracellular compartments where TOW resides, we performed immunolocalization to assess co-localization between TOW-GFP and various organelle markers.

TOW-GFP showed strong co-localization with clathrin heavy chain (CHC; a TGN marker) (Figure 5A), VHAa1 (a TGN and early endosome marker) (Figure 5B), and γCOP (a Golgi marker) (Figure 5C), but not with KDEL-containing proteins (an endoplasmic reticulum [ER] marker) (Figure 5D). Quantitative analysis using Pearson correlation and overlap coefficient confirmed significant overlap between TOW-GFP and CHC, VHAa1, and γCOP, but not with KDEL (Figure 5E). These findings demonstrate that TOW localizes to the PM, *trans*-Golgi network (TGN), and Golgi, aligning with key steps in PIN trafficking routes and reinforcing TOW involvement in the regulation of PIN trafficking.

TOW physically interacts with RLKs involved in auxin canalization

Several RLKs, including CAMEL, CANAR, and TMK1, are well-established components of PIN1-dependent auxin canalization.[2] CAMEL, a direct TOW, functions together with its interactor CANAR as a receptor complex that modulates PIN polarization and auxin flow.[12] Similarly, TMK1, a co-receptor of the auxin receptor ABP1, plays an essential role in auxin-guided

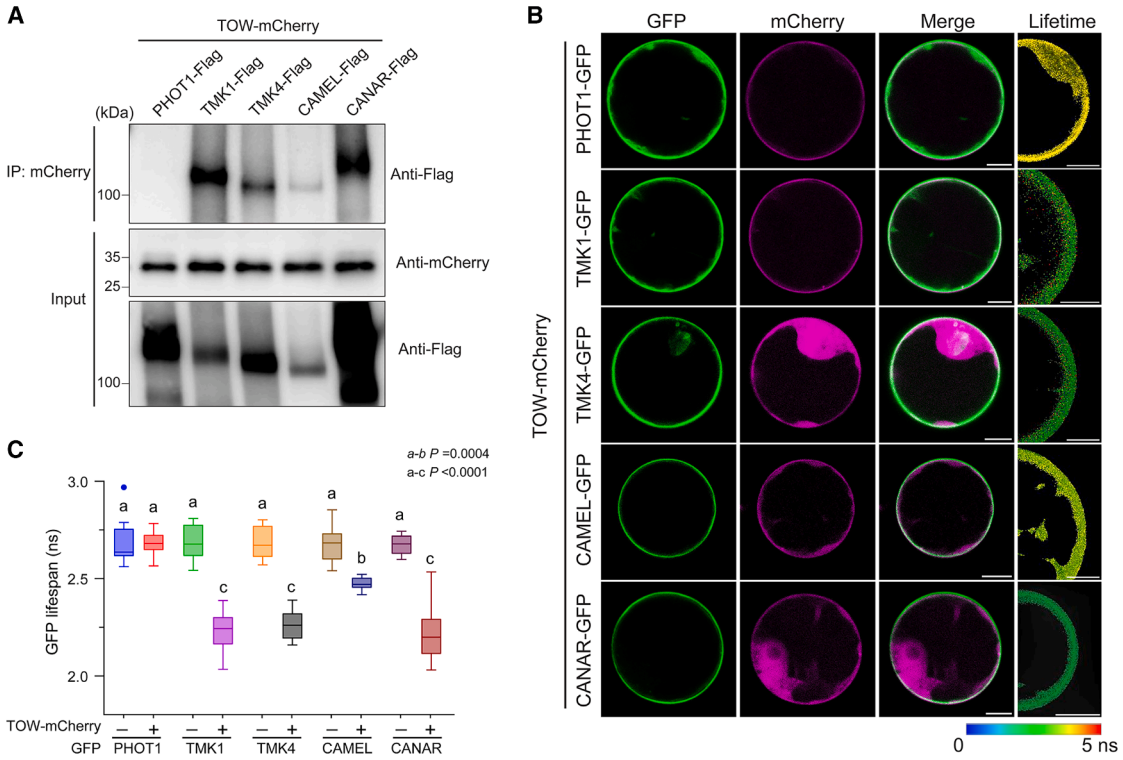

Figure 6. Physical interaction between TOW and RLKs involved in auxin canalization

(A) Co-immunoprecipitation (coIP) assay showing the interaction between TOW and RLKs (PHOT1, TMK1, TMK4, CAMEL, and CANAR) in *Nicotiana benthamiana*. mCherry-tagged TOW and FLAG-tagged RLKs were transiently co-expressed. Total protein extracts were immunoblotted with anti-RFP and anti-FLAG antibodies to assess input levels. CoIP was performed using anti-RFP antibody, and co-precipitated FLAG-tagged RLKs were detected by immunoblotting with anti-FLAG. The image shown is representative of two biological replicates.

(B and C) FRET-FLIM analysis of transiently expressed *35S::TOW-mCherry* and *35S::RLKs-GFP* in Arabidopsis protoplasts. GFP fluorescence lifetime was calculated from manually selected regions of interest (ROIs) across at least 10 individual protoplast cells. Heatmaps show fluorescence lifetime values. Data are presented as Tukey boxplots from three independent experiments, and one representative experiment is shown. Statistical significance was determined using one-way ANOVA followed by Tukey's post hoc test.

vascular development.[15] These RLKs most likely regulate PIN polarity through phosphorylation. Notably, TOW shares overlapping subcellular localization and mutant phenotypes with these RLKs, suggesting a potential functional relationship.

To examine whether TOW physically associates with these RLKs, we co-expressed mCherry-tagged TOW with FLAG-tagged TMK1, TMK4, CAMEL, and CANAR in *Nicotiana benthamiana*. Phototropin 1 (PHOT1) was included as a negative control, being also a PM-localized kinase but not linked to auxin canalization.[26,27] Co-immunoprecipitation using anti-RFP beads showed that TOW interacted with TMK1, TMK4, CAMEL, and CANAR, but not with PHOT1 (Figure 6A).

To further validate and quantify these interactions, we performed Förster resonance energy transfer coupled with fluorescence lifetime imaging microscopy (FRET-FLIM) in *Arabidopsis* protoplasts. Co-expression of *35S::TOW-mCherry* with GFP-tagged TMK1, TMK4, CAMEL, and CANAR resulted in a significant reduction in GFP fluorescence lifetime compared with the corresponding RLK-GFP proteins expressed alone (Figure 6C), indicating physical interaction. Spatially resolved FRET-FLIM analysis confirmed that these interactions occur at the cell surface (Figure 6B). Notably, the GFP fluorescence lifetime of PHOT1-GFP remained unaffected by TOW-mCherry co-expression (Figure 6C), confirming the specificity of TOW's interaction with canalization-associated RLKs.

These results demonstrate that TOW physically interacts with key RLK components, namely the CAMEL-CANAR complex, TMK1, and TMK4, of cell surface auxin perception, all involved in auxin canalization, suggesting that TOW may act within the same signaling modules to regulate auxin-mediated PIN polarity in auxin canalization processes.

TOW promotes PIN1-RLK interactions and stabilizes PIN1 localization at PM

To investigate whether TOW modulates the interaction between PIN1 and RLKs, we performed co-immunoprecipitation assays in *Nicotiana benthamiana* leaves transiently expressing the PIN1 hydrophilic loop ($PIN1^{HL}$) together with RLKs, in the presence or absence of TOW. Without TOW, $PIN1^{HL}$ exhibited strong interaction with TMK1 and CANAR, relatively weaker association with TMK4 and CAMEL, and no detectable interaction with PHOT1. Co-expression of TOW-Myc significantly enhanced the interaction of $PIN1^{HL}$ with TMK1, TMK4, CAMEL, and CANAR, while the absence of PHOT1 interaction remained

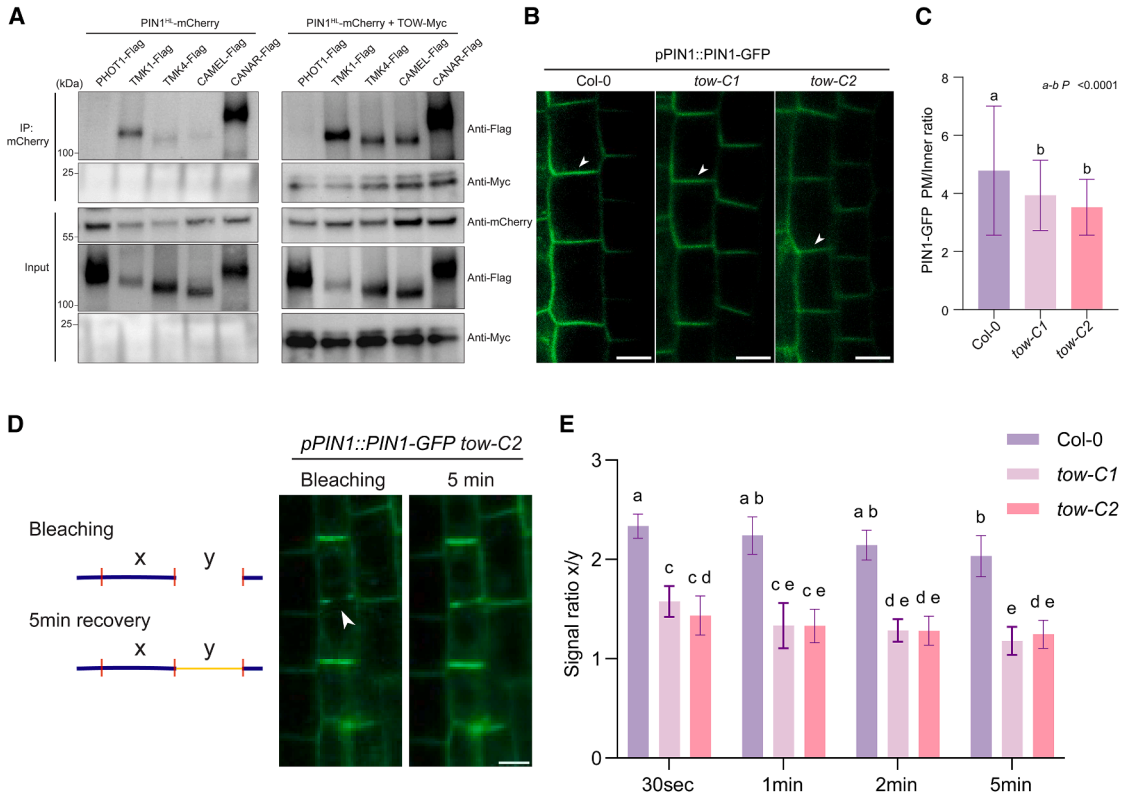

Figure 7. TOW promotes PIN1-RLK interactions and stabilizes PIN1 at PM

(A) Co-immunoprecipitation (coIP) assay showing interactions between the PIN1 hydrophilic loop (PIN1^{HL}) and RLKs in the presence or absence of TOW in *Nicotiana benthamiana*. mCherry-tagged PIN1^{HL}, FLAG-tagged RLKs, and Myc-tagged TOW were transiently co-expressed. Total protein extracts were immunoblotted with anti-RFP, anti-FLAG, and anti-Myc antibodies, respectively, to verify protein expression. CoIP was performed using an anti-RFP antibody, and co-precipitated RLKs were detected with anti-FLAG. The image shown is representative of two independent biological replicates.

(B) Subcellular localization of PIN1-GFP in the root endodermis of Col-0 and *tow* mutants. Scale bars, 10 μm.

(C) Quantification of relative fluorescence intensities in (B) showing reduced PM localization of PIN1-GFP in *tow* mutants. Data are presented as mean ± SD from three independent experiments, and one representative experiment is shown. Statistical significance was determined using one-way ANOVA followed by Tukey's post hoc test. Different letters indicate significant differences ($p < 0.05$). $n > 100$ cells per genotype.

(D) Fluorescence recovery after photobleaching (FRAP) analysis of PIN1-GFP dynamics. The lateral diffusion rate was estimated using the ratio of non-bleached to bleached membrane signal intensities. Bleached regions are indicated by arrowheads. Scale bars, 10 μm.

(E) Quantification of fluorescence recovery in (D) showing accelerated recovery of PIN1-GFP in *tow* mutants compared with Col-0. Data represent mean ± SD ($n = 10$). Statistical significance was determined using two-way ANOVA followed by Tukey's post hoc test.

See also Figure S5 and Table S2.

unchanged (Figure 7A). These findings suggest that TOW promotes and stabilizes the interaction between PIN1 and specific RLKs, potentially functioning as a scaffold protein within these complexes.

To determine whether TOW facilitates PIN1-RLK interactions by stabilizing PM-localized PIN1, we examined the subcellular localization of pPIN1::PIN1-GFP in *tow* mutants. Both *tow-C1* and *tow-C2* showed visibly reduced PM localization of PIN1-GFP in root endodermal cells compared with Col-0 (Figure 7B). Quantitative analysis of the PM-to-cytoplasm fluorescence ratio confirmed the significant reduction in both mutant alleles (Figure 7C), indicating that TOW contributes to maintaining PIN1 localization at the PM.

Next, we assessed the dynamic behavior of PIN1 in *tow* mutants using fluorescence recovery after photobleaching (FRAP). Following bleaching of a small PM region, the lateral diffusion rate of PIN1 was monitored by comparing the fluorescence intensity of bleached and non-bleached PM areas (Figure 7D). In Col-0, PIN1-GFP fluorescence gradually recovered over 5 min (Figure 7E). By contrast, *tow-C1* and *tow-C2* mutants exhibited significantly faster recovery, indicating an accelerated diffusion rate of PM-localized PIN1 (Figures 7D and 7E). Such rapid PIN1 recovery suggests an increased turnover of PIN1 at the PM in the absence of functional TOW, consistent with reduced PM stability and increased intracellular accumulation in *tow* mutants (Figures 7B and 7C). Moreover, we performed whole-cell FRAP to monitor *de novo* PIN1 delivery to the PM. After whole-cell bleaching, PIN1-GFP fluorescence gradually recovered over 2 h in all genotypes (Figure S5A). However, recovery rates were consistently lower in *tow-C1* and *tow-C2* compared with Col-0 (Figure S5B), suggesting a diminished capacity to restore newly synthesized PIN1 at the PM. Together, these results indicate that TOW restricts lateral PIN diffusion within the PM and likely limits endocytic internalization, thereby

stabilizing PIN1 at the PM. Alternatively, though less likely, TOW may promote the secretion of newly synthesized PIN1 and its recycling to the PM.

PIN phosphorylation is a well-established mechanism regulating PIN activity and polar localization,[28] and previous studies have shown that PIN phosphorylation is closely associated with vascular regeneration and the formation of polarized auxin transport channels.[12,15,17,29] To assess whether TOW influences the phosphorylation status of PIN proteins during auxin canalization, we performed phosphoproteomic analysis on 5-day-old Col-0, *tow-C2*, and *35S::TOW-GFP* seedlings. In total, we identified 1,719 phosphoproteins in Col-0, 2,003 in *tow-C2*, and 1,397 in *35S::TOW-GFP*, with substantial overlap among the three genotypes: 62.8% in Col-0, 53.7% in *tow-C2*, and 77.2% in *35S::TOW-GFP* (Figure S5C). After excluding methionine oxidation variants, we detected 2,815 distinct phospho-peptidoforms, which correspond to 2,116 unique peptide sequences. These included 11 PIN2 peptidoforms (10 sites across 4 clusters of adjacent residues), one for PIN1 and two for PIN3 (two adjacent sites) (Table S2). Notably, no significant differences in PIN protein phosphorylation levels were observed among the three genotypes (Figures S5D and S5E), indicating that loss or overexpression of TOW could not directly alter the phosphorylation status of PIN proteins.

Collectively, these findings indicate that TOW enhances the physical association between PIN1 and specific RLKs but has limited capacity to modulate PIN phosphorylation dynamics.

DISCUSSION

Spontaneous and self-organized formation of directional auxin transport channels provides positional information for the flexible formation of vasculature. The underlying canalization hypothesis proposes positive feedback between auxin and PIN auxin transporters as a key prerequisite. In this study, we identify TOW, a previously uncharacterized membrane protein, as a novel component of the auxin canalization machinery. Specifically, TOW functions as an essential component of auxin channel formation in the tissues, and at the levels of individual cells, it mediates correct PIN polarity and endocytic trafficking.

TOW has been identified as an auxin-inducible gene being transcriptionally regulated downstream of both TIR1/AFB-Aux/IAA-ARF canonical auxin signaling and the WRKY23 transcription factor. We show that indeed both ARFs and WRKY23 individually regulate TOW promoter activity (Figure 1C). Accordingly, *TOW* is expressed in developing vasculature (Figures 1F–1H) associated with increased auxin levels and transport and resembling the *WRKY23::GUS* expression pattern.[8] This spatial overlap reinforces the role of TOW in auxin-mediated developmental processes as a part of a conserved auxin canalization module downstream of WRKY23.

Functionally, TOW is required for auxin canalization-related processes, including regeneration and *de novo* formation of vasculature from the local auxin source, and also for the formation of auxin channels during these processes (Figures 2 and 3). Defects in these processes in *tow* mutants are comparable to those observed in *tmk*,[15] *camel*, and *canar*[12] mutants. At the level of individual cells, TOW, again similarly as shown for CAMEL and CANAR,[12] is involved in coordinated, auxin-induced PIN polarization (Figure 4). These commonalities support the idea that TOW functions within the same auxin canalization mechanism as these RLKs. As a comparison, ARF5/MONOPTEROS (MP) has been proposed to regulate plant self-organization.[30,31] Similar to TOW, MP acts downstream of TIR1-mediated auxin perception and is required for leaf vein patterning. However, unlike TOW, MP regulates PIN transcription, and *mp*, as well as other auxin signaling mutants, displays more severe leaf venation defects than those typically observed in mutants affecting auxin canalization components.[30] By contrast, TOW has effects on PIN trafficking and polarity by stabilizing the PIN1-RLK complex (Figure 7).

Our data further indicate that TOW modulates BFA-sensitive endocytic trafficking of PIN proteins. This was supported by the subcellular localization of TOW in the key compartments for vesicle sorting and recycling (Figure 5) and increased BFA-induced intracellular PIN accumulation in *tow* mutants (Figures 4 and S4). Interestingly, this trafficking defect manifested only after BFA treatment but was largely eliminated when co-treated with auxin. By contrast, aminophospholipid ATPase3 (ALA3), a phospholipid flippase previously shown to regulate PIN polarity and vesicle formation,[32] exhibits trafficking defects under all conditions, indicating that ALA3 functions as a general trafficking factor, whereas TOW appears to act more selectively, potentially downstream or in parallel to auxin regulation.

TOW encodes a small membrane protein of unknown function, and its mechanistic role in canalization remains mysterious. Notably, TOW physically associates with CAMEL, CANAR, and TMK1/4, all RLKs known to coordinate PIN phosphorylation and polarity required for canalization (Figure 6). Importantly, TOW enhances the interaction of these RLKs with PIN1 (Figure 7A). Given that TMK1 and the CAMEL-CANAR complex regulate PIN polarity via phosphorylation,[12,15,17,29] TOW may act as a scaffold or stabilizer facilitating PIN1-RLK complexes, modulate their activity, or function downstream as an effector of their signaling cascade. Supporting this, our FRAP analyses revealed that PM-localized PIN1 exhibits increased lateral diffusion and turnover in *tow* mutants (Figures 7D, 7E, S5A, and S5B), indicating that TOW primarily restricts lateral diffusion and endocytic internalization of PIN1 rather than affecting its delivery to the PM. Notably, no significant differences in PIN phosphorylation were detected in the presence or absence of TOW (Figures S5D and S5E), suggesting that TOW does not directly regulate PIN phosphorylation. Together, these findings support a model in which TOW stabilizes PIN1 at the PM, facilitating interactions with specific RLKs and thereby contributing to proper canalization, without directly altering PIN phosphorylation.

TOW's broader localization in endomembranes and its role in PIN trafficking suggest that TOW might serve as a functional bridge between RLK-mediated signaling at the PM and PIN endocytic trafficking. While RLKs such as CAMEL and CANAR likely act through phosphorylation to control PIN localization, TOW appears to translate these upstream signals into trafficking events, especially those regulated by auxin. This unique positioning would allow TOW to ensure the spatial and temporal precision of PIN trafficking necessary for effective polarization of auxin transport for canalization.

In summary, TOW emerges as a novel component involved in auxin canalization. It is extensively regulated downstream of the TIR1/AFB-Aux/IAA-WRKY23 intracellular auxin signaling pathway, while also interacting with TMK1, a key component of cell surface auxin signaling, as well as with the established PM canalization complex CAMEL-CANAR. Although its precise molecular function remains elusive, TOW likely mediates input from canonical transcriptional signaling and links cell surface auxin perception with PIN endocytic trafficking, thereby coordinating polarized PIN delivery to the PM—a mechanism proposed for auxin canalization by modeling approaches.[33] Future studies should focus on elucidating the molecular function of TOW, identifying its functional domains, expanding the characterization of its interactome, and uncovering the nature of mutual regulation between TOW and its associated receptor-like kinases.

RESOURCE AVAILABILITY

Lead contact

Further information and requests for resources and reagents should be directed to and will be fulfilled by the lead contact, Jiri Friml (jiri.friml@ist.ac.at).

Materials availability

Constructs and reagents in this study will be made available upon request, but a completed materials transfer agreement may be required if there is potential for commercial application.

Data and code availability

- The mass spectrometry proteomics data have been deposited to the ProteomeXchange[34] Consortium via the PRIDE[35] partner repository with the dataset identifier ProteomeXchange: PXD070189 and are publicly available as of the date of publication.
- This paper does not report original code.
- Any additional information required to reanalyze the data reported in this paper is available from the lead contact upon request.

ACKNOWLEDGMENTS

We thank Dr. Z. Ge (ISTA) for providing vectors for the CRISPR-Cas9 system, Dr. Armel Nicolas and Dr. Bella Bruszel for phosphoproteomic analysis, Prof. Michael Wrzaczek (Czech Academy of Sciences, Czechia) for valuable suggestions, and Prof. Maciek Adamowski (University of Gdańsk) for technical assistance. We also acknowledge the support of the Mass Spectrometry and Proteomics Facility, the Imaging & Optics Facility, and the Lab Support Facility at the Institute of Science and Technology Austria. This research was supported by the Scientific Service Units (SSU) of ISTA, utilizing resources provided by the Imaging & Optics Facility (IOF) and the Lab Support Facility (LSF). The work conducted by the Friml group was funded by the European Research Council (ERC) under grant agreement no. 101142681 (CYNIPS) and by the Austrian Science Fund (FWF) under project ESP271. We acknowledge the core facility CELLIM supported by MEYS CR (LM2023050 Czech-BioImaging) and the Plant Sciences Core Facility of CEITEC Masaryk University. E.M. received support from the National Science Centre (NCN), Poland, through the OPUS call within the Weave programme (grant no. 2021/43/I/NZ1/01835). T.N. received support from TowArds Next GENeration Crops, reg. no. CZ.02.01.01/00/22_008/0004581 of the ERDF Programme Johannes Amos Comenius.

AUTHOR CONTRIBUTIONS

Conceptualization, M.L. and J.F.; methodology, M.L. and J.F.; investigation, M.L., N.R., G.M., and E.M.; writing – original draft, M.L. and J.F.; writing – review & editing, M.L. and J.F.; funding acquisition and resources, M.L. and J.F.; supervision, M.L. and J.F.

DECLARATION OF INTERESTS

The authors declare no competing interests.

STAR★METHODS

Detailed methods are provided in the online version of this paper and include the following:

- KEY RESOURCES TABLE
- EXPERIMENTAL MODEL AND STUDY PARTICIPANT DETAILS
- METHOD DETAILS
  - Plasmid Construction
  - Quantitative Reverse-transcription PCR
  - TOW Promoter Activation and Dual Luciferase Assay
  - *in situ* immunolocalization
  - Cotyledon Vasculature Analysis
  - Local Auxin Application and Vascular Regeneration Experiments in Arabidopsis Stems
  - Förster Resonance Energy Transfer with Fluorescence Lifetime Imaging Microscopy (FRET-FLIM)
  - Co-Immunoprecipitation Assay
  - Phosphoproteomics Analysis
- QUANTIFICATION AND STATISTICAL ANALYSIS

SUPPLEMENTAL INFORMATION

Supplemental information can be found online at https://doi.org/10.1016/j.cub.2026.02.023.

Received: June 10, 2025
Revised: January 16, 2026
Accepted: February 16, 2026
Published: March 13, 2026

REFERENCES

1. Sachs, T. (1975). The induction of transport channels by auxin. Planta *127*, 201–206. https://doi.org/10.1007/BF00380716.
2. Hajný, J., Tan, S., and Friml, J. (2022). Auxin canalization: From speculative models toward molecular players. Curr. Opin. Plant Biol. *65*, 102174. https://doi.org/10.1016/j.pbi.2022.102174.
3. Bennett, T., Hines, G., and Leyser, O. (2014). Canalization: what the flux? Trends Genet. *30*, 41–48. https://doi.org/10.1016/j.tig.2013.11.001.
4. Luschnig, C., and Friml, J. (2024). Over 25 years of decrypting PIN-mediated plant development. Nat. Commun. *15*, 9904. https://doi.org/10.1038/s41467-024-54240-y.
5. Sauer, M., Balla, J., Luschnig, C., Wiśniewska, J., Reinöhl, V., Friml, J., and Benková, E. (2006). Canalization of auxin flow by Aux/IAA-ARF-dependent feedback regulation of PIN polarity. Genes Dev. *20*, 2902–2911. https://doi.org/10.1101/gad.390806.
6. Glanc, M., Fendrych, M., and Friml, J. (2018). Mechanistic framework for cell-intrinsic re-establishment of PIN2 polarity after cell division. Nat. Plants *4*, 1082–1088. https://doi.org/10.1038/s41477-018-0318-3.
7. Glanc, M., Van Gelderen, K., Hoermayer, L., Tan, S., Naramoto, S., Zhang, X., Domjan, D., Včelařová, L., Hauschild, R., Johnson, A., et al. (2021). AGC kinases and MAB4/MEL proteins maintain PIN polarity by limiting lateral diffusion in plant cells. Curr. Biol. *31*, 1918–1930.e5. https://doi.org/10.1016/j.cub.2021.02.028.
8. Prát, T., Hajný, J., Grunewald, W., Vasileva, M., Molnár, G., Tejos, R., Schmid, M., Sauer, M., and Friml, J. (2018). WRKY23 is a component of the transcriptional network mediating auxin feedback on PIN polarity. PLoS Genet. *14*, e1007177. https://doi.org/10.1371/journal.pgen.1007177.

9. Balla, J., Kalousek, P., Reinöhl, V., Friml, J., and Procházka, S. (2011). Competitive canalization of PIN-dependent auxin flow from axillary buds controls pea bud outgrowth. Plant J. *65*, 571–577. https://doi.org/10.1111/j.1365-313X.2010.04443.x.

10. Mazur, E., Benková, E., and Friml, J. (2016). Vascular cambium regeneration and vessel formation in wounded inflorescence stems of Arabidopsis. Sci. Rep. *6*, 33754. https://doi.org/10.1038/srep33754.

11. Tejos, R., Rodriguez-Furlán, C., Adamowski, M., Sauer, M., Norambuena, L., and Friml, J. (2018). PATELLINS are regulators of auxin-mediated PIN1 relocation and plant development in Arabidopsis thaliana. J. Cell Sci. *131*, jcs204198. https://doi.org/10.1242/jcs.204198.

12. Hajný, J., Prát, T., Rydza, N., Rodriguez, L., Tan, S., Verstraeten, I., Domjan, D., Mazur, E., Smakowska-Luzan, E., Smet, W., et al. (2020). Receptor kinase module targets PIN-dependent auxin transport during canalization. Science *370*, 550–557. https://doi.org/10.1126/science.aba3178.

13. Vanneste, S., Pei, Y., and Friml, J. (2025). Mechanisms of auxin action in plant growth and development. Nat. Rev. Mol. Cell Biol. *26*, 648–666. https://doi.org/10.1038/s41580-025-00851-2.

14. Mazur, E., Kulik, I., Hajný, J., and Friml, J. (2020). Auxin canalization and vascular tissue formation by TIR1/AFB-mediated auxin signaling in Arabidopsis. New Phytol. *226*, 1375–1383. https://doi.org/10.1111/nph.16446.

15. Friml, J., Gallei, M., Gelová, Z., Johnson, A., Mazur, E., Monzer, A., Rodriguez, L., Roosjen, M., Verstraeten, I., Živanović, B.D., et al. (2022). ABP1–TMK auxin perception for global phosphorylation and auxin canalization. Nature *609*, 575–581. https://doi.org/10.1038/s41586-022-05187-x.

16. Huang, R., Wang, J., Chang, M., Tang, W., Yu, Y., Zhang, Y., Peng, Y., Wang, Y., Guo, Y., Lu, T., et al. (2026). TMK-PIN1 drives a short self-organizing circuit for auxin export and signaling in Arabidopsis. Dev Cell *61*, 73–84.e6.

17. Rodriguez, L., Fiedler, L., Zou, M., Giannini, C., Monzer, A., Vladimirtsev, D., Randuch, M., Yu, Y., Gelová, Z., Verstraeten, I., et al. (2025). ABP1/ABL3-TMK1 cell-surface auxin signaling targets PIN2-mediated auxin fluxes for root gravitropism. Cell *188*, 6138–6150.e17. https://doi.org/10.1016/j.cell.2025.08.026.

18. Okushima, Y., Overvoorde, P.J., Arima, K., Alonso, J.M., Chan, A., Chang, C., Ecker, J.R., Hughes, B., Lui, A., Nguyen, D., et al. (2005). Functional genomic analysis of the AUXIN RESPONSE FACTOR gene family members in Arabidopsis thaliana: unique and overlapping functions of ARF7 and ARF19. Plant Cell *17*, 444–463. https://doi.org/10.1105/tpc.104.028316.

19. Christensen, S.K., Dagenais, N., Chory, J., and Weigel, D. (2000). Regulation of auxin response by the protein kinase PINOID. Cell *100*, 469–478. https://doi.org/10.1016/S0092-8674(00)80682-0.

20. Friml, J., Yang, X., Michniewicz, M., Weijers, D., Quint, A., Tietz, O., Benjamins, R., Ouwerkerk, P.B.F., Ljung, K., Sandberg, G., et al. (2004). A PINOID-dependent binary switch in apical-basal PIN polar targeting directs auxin efflux. Science *306*, 862–865. https://doi.org/10.1126/science.1100618.

21. Khan, A., Fornes, O., Stigliani, A., Gheorghe, M., Castro-Mondragon, J.A., van der Lee, R., Bessy, A., Chèneby, J., Kulkarni, S.R., Tan, G., et al. (2018). JASPAR 2018: update of the open-access database of transcription factor binding profiles and its web framework. Nucleic Acids Res. *46*, D260–D266. https://doi.org/10.1093/nar/gkx1126.

22. Scarpella, E., Marcos, D., Friml, J., and Berleth, T. (2006). Control of leaf vascular patterning by polar auxin transport. Genes Dev. *20*, 1015–1027. https://doi.org/10.1101/gad.1402406.

23. Balla, J., Medveďová, Z., Kalousek, P., Matiješčuková, N., Friml, J., Reinöhl, V., and Procházka, S. (2016). Auxin flow-mediated competition between axillary buds to restore apical dominance. Sci. Rep. *6*, 35955. https://doi.org/10.1038/srep35955.

24. Geldner, N., Friml, J., Stierhof, Y.D., Jürgens, G., and Palme, K. (2001). Auxin transport inhibitors block PIN1 cycling and vesicle trafficking. Nature *413*, 425–428. https://doi.org/10.1038/35096571.

25. Paciorek, T., Zazímalová, E., Ruthardt, N., Petrásek, J., Stierhof, Y.-D., Kleine-Vehn, J., Morris, D.A., Emans, N., Jürgens, G., Geldner, N., et al. (2005). Auxin inhibits endocytosis and promotes its own efflux from cells. Nature *435*, 1251–1256. https://doi.org/10.1038/nature03633.

26. Sakamoto, K., and Briggs, W.R. (2002). Cellular and subcellular localization of phototropin 1. Plant Cell *14*, 1723–1735. https://doi.org/10.1105/tpc.003293.

27. Christie, J.M., Yang, H., Richter, G.L., Sullivan, S., Thomson, C.E., Lin, J., Titapiwatanakun, B., Ennis, M., Kaiserli, E., Lee, O.R., et al. (2011). phot1 inhibition of ABCB19 primes lateral auxin fluxes in the shoot apex required for phototropism. PLoS Biol. *9*, e1001076. https://doi.org/10.1371/journal.pbio.1001076.

28. Tan, S., Luschnig, C., and Friml, J. (2021). Pho-view of auxin: reversible protein phosphorylation in auxin biosynthesis, transport and signaling. Mol. Plant *14*, 151–165. https://doi.org/10.1016/j.molp.2020.11.004.

29. Huang, R., Wang, J., Chang, M., Tang, W., Yu, Y., Zhang, Y., Peng, Y., Wang, Y., Guo, Y., Lu, T., et al. (2025). TMK-PIN1 drives a short self-organizing circuit for auxin export and signaling in Arabidopsis. Dev. Cell *61*, 73–84.e6. https://doi.org/10.1016/j.devcel.2025.09.009.

30. Krogan, N.T., Marcos, D., Weiner, A.I., and Berleth, T. (2016). The auxin response factor MONOPTEROS controls meristem function and organogenesis in both the shoot and root through the direct regulation of PIN genes. New Phytol. *212*, 42–50. https://doi.org/10.1111/nph.14107.

31. Bhatia, N., Bozorg, B., Larsson, A., Ohno, C., Jönsson, H., and Heisler, M.G. (2016). Auxin acts through MONOPTEROS to regulate plant cell polarity and pattern phyllotaxis. Curr. Biol. *26*, 3202–3208. https://doi.org/10.1016/j.cub.2016.09.044.

32. Zhang, X., Adamowski, M., Marhava, P., Tan, S., Zhang, Y., Rodriguez, L., Zwiewka, M., Pukyšová, V., Sánchez, A.S., Raxwal, V.K., et al. (2020). Arabidopsis flippases cooperate with ARF GTPase exchange factors to regulate the trafficking and polarity of PIN auxin transporters. Plant Cell *32*, 1644–1664. https://doi.org/10.1105/tpc.19.00869.

33. Wabnik, K., Kleine-Vehn, J., Balla, J., Sauer, M., Naramoto, S., Reinöhl, V., Merks, R.M.H., Govaerts, W., and Friml, J. (2010). Emergence of tissue polarization from synergy of intracellular and extracellular auxin signaling. Mol. Syst. Biol. *6*, 447. https://doi.org/10.1038/msb.2010.103.

34. Deutsch, E.W., Bandeira, N., Perez-Riverol, Y., Sharma, V., Carver, J.J., Mendoza, L., Kundu, D.J., Wang, S., Bandla, C., Kamatchinathan, S., et al. (2023). The ProteomeXchange consortium at 10 years: 2023 update. Nucleic Acids Res. *51*, D1539–D1548. https://doi.org/10.1093/nar/gkac1040.

35. Perez-Riverol, Y., Bandla, C., Kundu, D.J., Kamatchinathan, S., Bai, J., Hewapathirana, S., John, N.S., Prakash, A., Walzer, M., Wang, S., et al. (2025). The PRIDE database at 20 years: 2025 update. Nucleic Acids Res. *53*, D543–D553. https://doi.org/10.1093/nar/gkae1011.

36. Benková, E., Michniewicz, M., Sauer, M., Teichmann, T., Seifertová, D., Jürgens, G., and Friml, J. (2003). Local, efflux-dependent auxin gradients as a common module for plant organ formation. Cell *115*, 591–602. https://doi.org/10.1016/S0092-8674(03)00924-3.

37. Schneider, C.A., Rasband, W.S., and Eliceiri, K.W. (2012). NIH Image to ImageJ: 25 years of image analysis. Nat. Methods *9*, 671–675. https://doi.org/10.1038/nmeth.2089.

38. Rauluseviciute, I., Riudavets-Puig, R., Blanc-Mathieu, R., Castro-Mondragon, J.A., Ferenc, K., Kumar, V., Lemma, R.B., Lucas, J., Chèneby, J., Baranasic, D., et al. (2024). JASPAR 2024: 20th anniversary of the open-access database of transcription factor binding profiles. Nucleic Acids Res. *52*, D174–D182. https://doi.org/10.1093/nar/gkad1059.

39. Letunic, I., and Bork, P. (2024). Interactive Tree of Life (iTOL) v6: recent updates to the phylogenetic tree display and annotation tool. Nucleic Acids Res. *52*, W78–W82. https://doi.org/10.1093/nar/gkae268.

40. Ge, Z., Zheng, L., Zhao, Y., Jiang, J., Zhang, E.J., Liu, T., Gu, H., and Qu, L.-J. (2019). Engineered xCas9 and SpCas9-NG variants broaden PAM recognition sites to generate mutations in Arabidopsis plants. Plant Biotechnol. J. *17*, 1865–1867. https://doi.org/10.1111/pbi.13148.

41. Li, L., Verstraeten, I., Roosjen, M., Takahashi, K., Rodriguez, L., Merrin, J., Chen, J., Shabala, L., Smet, W., Ren, H., et al. (2021). Cell surface and intracellular auxin signalling for H+ fluxes in root growth. Nature *599*, 273–277. https://doi.org/10.1038/s41586-021-04037-6.

42. Tan, S., Zhang, X., Kong, W., Yang, X.-L., Molnár, G., Vondráková, Z., Filepová, R., Petrášek, J., Friml, J., and Xue, H.-W. (2020). The lipid code-dependent phosphoswitch PDK1–D6PK activates PIN-mediated auxin efflux in Arabidopsis. Nat. Plants *6*, 556–569. https://doi.org/10.1038/s41477-020-0648-9.

43. Hellens, R.P., Allan, A.C., Friel, E.N., Bolitho, K., Grafton, K., Templeton, M.D., Karunairetnam, S., Gleave, A.P., and Laing, W.A. (2005). Transient expression vectors for functional genomics, quantification of promoter activity and RNA silencing in plants. Plant Methods *1*, 13. https://doi.org/10.1186/1746-4811-1-13.

44. Qi, L., Kwiatkowski, M., Chen, H., Hoermayer, L., Sinclair, S., Zou, M., Del Genio, C.I., Kubeš, M.F., Napier, R., Jaworski, K., et al. (2022). Adenylate cyclase activity of TIR1/AFB auxin receptors in plants. Nature *611*, 133–138. https://doi.org/10.1038/s41586-022-05369-7.

45. Mazur, E., Kurczyńska, E.U., and Friml, J. (2014). Cellular events during interfascicular cambium ontogenesis in inflorescence stems of Arabidopsis. Protoplasma *251*, 1125–1139. https://doi.org/10.1007/s00709-014-0620-5.

46. Thompson, J.D., Higgins, D.G., and Gibson, T.J. (1994). CLUSTAL W: improving the sensitivity of progressive multiple sequence alignment through sequence weighting, position-specific gap penalties and weight matrix choice. Nucleic Acids Res. *22*, 4673–4680. https://doi.org/10.1093/nar/22.22.4673.

47. Tamura, K., Stecher, G., and Kumar, S. (2021). MEGA11: molecular evolutionary genetics analysis version 11. Mol. Biol. Evol. *38*, 3022–3027. https://doi.org/10.1093/molbev/msab120.

STAR★METHODS

KEY RESOURCES TABLE

REAGENT or RESOURCE	SOURCE	IDENTIFIER
Antibodies		
anti-GFP antibody	Agrisera	Cat#AS20 4511; RRID:AB_1271075
anti-mCherry antibody	Abcam	Cat#ab167453; RRID:AB_2571870
anti-Flag antibody	Agrisera	Cat#AS16 3222;RRID:AB_10764132
anti-Myc antibody	Agrisera	Cat#AS21 4628; RRID:AB_11214006
Anti-Rabbit IgG HRP	ThermoFisher	Cat#31460; RRID:AB_1968815
anti-rabbit Cy3	Sigma-Aldrich	Cat#C2306; RRID:AB_1947003
anti-mouse Alexa Fluor 488	Sigma-Aldrich	Cat#A11029; RRID:AB_1101761
anti-PIN1 antibody	Lab stock	Hajný et al.[12]
anti-PIN2 antibody	Lab stock	Hajný et al.[12]
anti-CHC antibody	ThermoFisher	Cat#A304-743A; RRID:AB_2620938
anti-VHAa1 antibody	Agrisera	Cat#AS14 2822
anti-γCOP antibody	Agrisera	Cat#AS08 327
anti-KDEL antibody	Agrisera	Cat#AS08 325; RRID:AB_10693914
Bacterial and virus strains		
Escherichia coli (E. coli) DH5α competent cell	Lab stock / Invitrogen	Cat#18265017
Rhizobium radiobacter (Agrobacterium tumefaciens) GV3101 competent cell	Lab stock/ GoldBio	Cat#CC-207-5x50
Chemicals, peptides, and recombinant proteins		
IAA	Sigma-Aldrich	Cat#15148-2G
Acetosyringone	MCE	Cat#HY-W009884
MES	Duchefa	Cat#M1503
$MgCl_2$	Merck Chemicals	Cat#105833
DTT	Sigma-Aldrich	Cat#D0632
protease inhibitor cocktail	Sigma-Aldrich	Cat#11836170001
Igepal CA-630	Sigma-Aldrich	Cat#I3021
Deoxycholate	Sigma-Aldrich	Cat#D6750
RFP-Trap Magnetic Agarose	Chromotek	Cat#rtma
Luna Universal qPCR Master Mix	NEB	Cat#M3003S
Critical commercial assays		
RNeasy Plant Mini Kit	QIAGEN	Cat#74904
RevertAid First Strand cDNA Synthesis Kit	Thermo	Cat#K1622
Dual-Luciferase Reporter Assay System	Promega	Cat#E1910
E.Z.N.A. Plasmid Maxi Kit I	Omega BioTek	Cat#D6922-04
Deposited data		
Phosphoproteomics	This Paper	ProteomeXchange: PXD070189
Microarray data	Hajný et al.[12]	https://doi.org/10.1126/science.aba3178
Microarray data	Prát et al.[8]	https://doi.org/10.1371/journal.pgen.1007177.s006
Microarray data	Okushima et al.[18]	GEO: GSE627, GEO: GSM9571, GEO: GSM9594
Experimental models: Organisms/strains		
A. thaliana: Columbia-0 (Col-0)	NASC	N60000
A. thaliana: *arf7 arf19*	Hajný et al.[12]	N/A

(*Continued on next page*)

Continued		
REAGENT or RESOURCE	SOURCE	IDENTIFIER
A. thaliana: wrky23-1, 35S::WRKY23-GR	Prát et al.[8]	N/A
A. thaliana: pPIN1::PIN1-GFP	Benková et al.[36]	N/A
A. thaliana: *CRISPR tow*	This paper	N/A
A. thaliana: pPIN1::PIN1-GFP *tow*	This paper	N/A
A. thaliana: pTOW::TOW-GFP *tow*	This paper	N/A
A. thaliana: 35S::TOW-GFP	This paper	N/A
Oligonucleotides		
see Table S1	This paper	N/A
Recombinant DNA		
Plasmid: pTOW::TOW-GFP	This Paper	N/A
Plasmid: 35S::TOW-GFP	This Paper	N/A
Plasmid: 35S::TOW-Myc	This Paper	N/A
Plasmid: 35S::TOW-mCherry	This Paper	N/A
Plasmid: CRISPR tow-sgRNA	This Paper	N/A
Plasmid: pTOW::GUS	This Paper	N/A
Plasmid: pTOW::DUAL-LUC	This Paper	N/A
Plasmid: 35S::ARF7-HA	This Paper	N/A
Plasmid: 35S::ARF19-HA	This Paper	N/A
Plasmid: 35S::WRKY23-HA	This Paper	N/A
Plasmid: 35S::PIN1^{HL}-mCherry	This Paper	N/A
Plasmid: 35S::PHOT1-Flag	This Paper	N/A
Plasmid: 35S::TMK1-Flag	This Paper	N/A
Plasmid: 35S::TMK4-Flag	This Paper	N/A
Plasmid: 35S::CAMRL-Flag	This Paper	N/A
Plasmid: 35S::CANAR-Flag	This Paper	N/A
Plasmid: 35S::PHOT1-GFP	This Paper	N/A
Plasmid: 35S::TMK1-GFP	This Paper	N/A
Plasmid: 35S::TMK4-GFP	This Paper	N/A
Plasmid: 35S::CAMEL-GFP	This Paper	N/A
Plasmid: 35S::CANAR-GFP	This Paper	N/A
Software and algorithms		
ImageJ	Schneider et al.[37]	https://imagej.net/ij/
MEGA 11	The Pennsylvania State University	https://www.megasoftware.net/
GraphPad Prism 8	GraphPad	https://www.graphpad.com/
Consurf	The Tel Aviv University	https://consurf.tau.ac.il/
Phytozome 13	University of California	https://phytozome-next.jgi.doe.gov/
ClustalW	University College Dublin	http://www.clustal.org/clustal2/
JASPAR	Rauluseviciute et al.[38]	https://jaspar.elixir.no/
iTOL v6	Letunic and Bork[39]	https://itol.embl.de/

EXPERIMENTAL MODEL AND STUDY PARTICIPANT DETAILS

All *Arabidopsis thaliana* mutants and transgenic lines used in this study are in the Col-0 background. The *arf7 arf19* double mutant,[12] *wrky23-1* mutant[8] (SALK_003943), *35S::WRKY23-GR*,[8] and *pPIN1::PIN1-GFP*[36] have been described previously.

The *tow* mutants were generated using CRISPR-Cas9 technology.[40] To enhance editing efficiency, we designed two single-guide RNA (*sgRNA*) sequences targeting *TOW* (*AT3G09280*) gene. *Cas9-free* homozygous mutants were identified through hygromycin resistance screening and confirmed by direct sequencing of PCR products from T3 generation offspring. Four independent mutation events were selected for the test. The *wrky23 tow* double mutant was generated by crossing *wrky23-1* (SALK_003943) with *tow-C2*. Homozygous progeny was identified by genotyping and direct sequencing using the primers listed in Table S1.

To generate marker lines in the *tow* mutant background, *pPIN1::PIN1-GFP* seedlings were crossed with *tow* mutants. Homozygous offspring were selected through fluorescence screening and direct sequencing of PCR products from the T3 generation.

For complementary lines, a 2.5 kb genomic fragment containing the promoter and coding regions of *TOW* was amplified from genomic DNA and cloned into the pDONR221 vector. The resulting entry clones were recombined into the binary vector pB7FWG0 or pB7HAWG0 to generate *pTOW::TOW-GFP*. The final constructs were introduced into *A. tumefaciens GV3101* via electroporation, and subsequently transformed into *tow* mutants using the floral dip method.

To generate the *35S::TOW-GFP* transgenic line, the TOW coding sequence (CDS) without a stop codon was cloned into pDONR221 before being recombined into the destination vector pB7FWG2. The final constructs were then transformed into Col-0 using the floral dip method. All primers used for plasmid construction are listed in Table S1.

Seeds were surface-sterilized with chlorine gas, sown on AM+ medium containing half-strength Murashige and Skoog (0.5× MS), 1% (w/v) sucrose and 0.8% (w/v) phytoagar (pH 5.9), stratified in the dark at 4 °C for 2 days, and then grown vertically at 21 °C under a long-day photoperiod (16 h light/8 h dark). The light source consisted of Philips GreenPower LED production modules (deep red [660 nm]/far-red [720 nm]/blue [455 nm] combination, Philips) with a photon density[41] of 140.4 μmol m−2 s−1 ± 3%.

METHOD DETAILS

Plasmid Construction

For in planta expression, entry vectors containing the coding sequences of TMK1, CAMEL, CANAR, and TMK4[42] were recombined into the pB7ChWG2 binary vectors to generate C-terminal mCherry fusions. The CDS region of *ARF7, ARF19* and *WRKY23* were amplified and cloned into the pENTR/D-TOPO vector, respectively. The resulting entry clones were recombined into the binary vector pB7HAWG2 to generate *35S::ARF7-HA*, *35S::ARF19-HA* and *35S::WRKY23-HA*.

To construct the TOW promoter reporter, an entry vector carrying the 2,156 bp upstream fragment of the *TOW* gene was recombined into the dual luciferase reporter vector pGreenII 0800-LUC[43] to generate the *pTOW:DUAL-LUC* plant binary vector. Primers used for plasmid construction are listed in Table S1.

Quantitative Reverse-transcription PCR

RNA extraction, cDNA synthesis, and reverse transcription-quantitative PCR (RT-qPCR) were performed as described previously.[44] Briefly, five-day-old seedlings were transferred to AM+ liquid medium (mock) or medium containing IAA or DEX. Each treatment was performed in three biological replicates. Seedlings were collected at the indicated time points after treatment, and RNA was extracted using the RNeasy Plant Mini Kit (QIAGEN, 74904). One microgram of total RNA was used for reverse transcription after genomic DNA removal, following the instructions of the RevertAid First Strand cDNA Synthesis Kit (Thermo, K1622). cDNA was diluted 20-fold before RT-qPCR. Samples were pipetted in three technical replicates using an Automated Workstation Biomek i5 (Beckman Coulter). RT-qPCR was performed with a LightCycler 480 (Roche) using Luna Universal qPCR Master Mix (NEB, M3003S). Sequences of gene-specific primers are listed in Table S1. Relative gene expression levels were calculated using the *ΔΔCT* method, with *PROTEIN PHOSPHATASE 2A SUBUNIT A3 (PP2AA3)* as the internal control.

TOW Promoter Activation and Dual Luciferase Assay

For promoter activation assays, the *pTOW:DUAL-LUC* construct was transiently co-expressed in *Nicotiana benthamiana* with free HA or HA-fused *ARF7*, *ARF19*, and *WRKY23*. Specifically, *A. tumefaciens* GV3101 strains carrying expression constructs *35S::WRKY23-HA*, *35S::ARF7-HA*, *35S::ARF19-HA*, empty pB7HAWG2, and *pTOW:DUAL-LUC* were grown overnight in LB medium, pelleted by centrifugation, and resuspended in infiltration buffer (10 mM MES, 10 mM $MgCl_2$, and 200 μM acetosyringone) to an OD600 of 1.0. Equal volumes of different constructs were mixed for infiltration. Cultures were spot-infiltrated into four-week-old tobacco leaves. Leaf discs were collected two days after infiltration, ground in liquid nitrogen, and lysed with PLB buffer from the Dual-Luciferase Reporter Assay System (Promega, E1910). Lysates were centrifuged at 12,000 g for 1 min, and 10 μL of supernatant was used to measure FLUC and RLUC activities according to the manufacturer's instructions using a Victor3 plate reader (PerkinElmer). FLUC and RLUC substrates were added via an automatic injector at 25°C, followed by 2 s of shaking with a 2 s delay. Signals were captured for 3 s and recorded as counts per second. To quantify *TOW* promoter activity, the ratio of FLUC to RLUC activity was calculated for each combination.

in situ immunolocalization

Immunostaining in primary root was performed on three-day-old seedlings as previously described.[5] The primary antibodies used were rabbit *anti*-PIN1,[12] diluted 1:1,000 (v/v); rabbit *anti*-PIN2 diluted 1:1,000 (v/v),[12] mouse anti-GFP (cat. no. AS20 4511; AgriSera), diluted 1:5,000 (v/v); rabbit anti-CHC (cat. no. A304-743A, ThermoFisher), diluted 1:1,000 (v/v); rabbit *anti*-γCOP (cat. no. AS08 327; Agrisera) diluted 1:1,000 (v/v); rabbit anti-VHA a1 (cat. no. AS14 2822; Agrisera) diluted 1:1,000 (v/v); rabbit *anti*-KDEL (cat. no. AS08 325; Agrisera) diluted 1:1,000 (v/v). The secondary antibody used was sheep anti-rabbit conjugated with Cy3 (cat. no. C2306; Sigma-Aldrich), diluted 1:600 (v/v) and anti-mouse Alexa Fluor 488 (cat. no. A11029; Sigma-Aldrich), diluted 1:600 (v/v). For PIN1 immunolocalization in young leaves, tissues were cleared sequentially in methanol and ethanol/xylene solution after fixation, and subsequent procedures were carried out as described for roots.

Cotyledon Vasculature Analysis

Cotyledons of 10-day-old seedlings were harvested and incubated overnight in 70% ethanol for initial clearing. The samples were then transferred to a 4% (v/v) HCl and 20% (v/v) methanol solution and incubated at 65°C for 15 minutes, followed by incubation in a 7% (v/v) NaOH and 70% (v/v) ethanol solution at room temperature for 15 minutes.

To ensure gradual rehydration, cotyledons were sequentially transferred through an ethanol series of 70% (v/v), 50% (v/v), 25% (v/v), and 10% (v/v) ethanol, with each step lasting 5 minutes. The samples were then immersed in a 25% (v/v) glycerol and 5% (v/v) ethanol solution before being mounted in 50% (v/v) glycerol for imaging. Differential interference contrast (DIC) microscopy was performed using an Olympus BX53 microscope.

Local Auxin Application and Vascular Regeneration Experiments in Arabidopsis Stems

Young Arabidopsis plants with inflorescence stems at the primary tissue stage (vascular bundles separated by interfascicular parenchyma) were selected for a two-step experiment, as previously described.[10] First, the flowering parts of the stems were removed using a sharp razor blade, leaving a 7 cm-long stem. To stabilize the stems, they were attached to a polypropylene tube and subjected to a 2.5 g lead weight for six days, promoting the formation of a closed ring of cambium around the stem circumference.[45] Next, a transverse incision was made above the leaf rosette to disrupt the longitudinal cambium continuity and the basipetal transport of endogenous auxin. A droplet of lanolin paste containing IAA (Sigma-Aldrich, cat. no. 15148-2G) was then applied just below the cut. This setup ensured that any observed changes resulted solely from the externally applied auxin. The lanolin-IAA mixture was refreshed every two days throughout the experiment. Each experiment was conducted twice per plant line, with at least 10 plants analyzed per replicate. Finally, the samples were collected, manually sectioned, and mounted in a 50% glycerol aqueous solution for imaging.

Förster Resonance Energy Transfer with Fluorescence Lifetime Imaging Microscopy (FRET-FLIM)

Protoplasts were isolated from root cell suspension cultures as previously described.[12] Plasmids were prepared using the E.Z.N.A. Plasmid Maxi Kit I (Omega Bio-Tek). Protoplasts were transfected with 10 μg of plasmid DNA using the PEG-calcium-mediated transformation method and incubated in the dark at room temperature for 12–16 hr before imaging. FRET-FLIM measurements were performed using a Leica TCS SP8 confocal microscope equipped with a PicoQuant FLIM system. The donor fluorophore was excited at 488 nm using a 70% white-light laser source (10% intensity), and emission fluorescence was collected by a HyD detector with bandpass filters of 499–551 nm and 600–650 nm. The acceptor fluorophore was excited at 561 nm using the same 70% white-light laser source (50% intensity), and emission was collected using a 600–650 nm bandpass filter. Time-correlated single-photon counting (TCSPC) data acquisition was performed using PicoQuant SymPhoTime software, with an acquisition time of 60–120 seconds per image to ensure sufficient photon counts (>1,000 photons per pixel). A segmented line was drawn along the plasma membrane (PM) region to measure the mean signal intensity for each channel. Fluorescence decay curves were analyzed using Leica LAS X software, and lifetime values were extracted from at least 10 independent regions of interest (ROIs) per sample. Statistical significance was assessed using one-way ANOVA followed by Tukey's post hoc test in GraphPad Prism. To generate the FRET-SE efficiency heatmap, the corresponding ROIs were processed using the Image FLIM module in LAS X.

Co-Immunoprecipitation Assay

Co-immunoprecipitation assays were performed using *Nicotiana benthamiana*. Transfected protoplasts were lysed in 500 μL of lysis buffer (50 mM Tris-HCl, pH 7.4, 150 mM NaCl, 1 mM DTT, 1× protease inhibitor cocktail (cat. no. 11836170001, Sigma-Aldrich)). The membrane fraction was isolated by flash-freezing the protoplasts in liquid nitrogen, thawing on ice, and centrifuging at 14,000 *g* at 4°C for 45 minutes. The supernatant was discarded, and the pellet was resuspended in lysis buffer supplemented with 0.5% NP-40. The sample was then centrifuged at 12,000 *g* at 4°C for 15 minutes, and the supernatant was collected for co-immunoprecipitation. For co-immunoprecipitation, the membrane fractions were incubated with anti-RFP beads (Chromotek; cat. no. rtma) for 1 hr at 4°C. The immunoprecipitated proteins were washed four times with Washing Buffer 1 (150 mM NaCl, 1% Igepal CA-630, 0.5% sodium deoxycholate, 0.1% SDS, 50 mM Tris-HCl, pH 8.0) and once with Washing Buffer 2 (20 mM Tris-HCl, pH 7.5). Proteins were eluted from the beads using preheated elution buffer (50 mM Tris-HCl, pH 6.8, 50 mM DTT, 1% SDS, 1 mM EDTA, 0.005% bromophenol blue, and 10% glycerol) at 95°C. Eluted proteins were separated by 10% (v/v) SDS-PAGE and detected using an anti-mCherry antibody (1:5,000 dilution, cat. no. ab167453, Abcam), anti-Flag-HRP antibody (1:10,000 dilution, cat. no. AS16 3222, Agrisera), or anti-Myc-HRP (1:5,000 dilution, cat. no. AS21 4628, Agrisera).

Phosphoproteomics Analysis

Samples preparation

Roots of 5-d-old seedlings of Col-0, *tow-C2 and 35S::TOW-GFP* were collected and ground into fine powder in liquid nitrogen. Samples were first cleaned up by SP3 using a commercial kit (PreOmics GmbH, 100 mg of beads per sample), then processed using the iST kit (PreOmics GmbH) according to the manufacturer's instructions. Tryptic digestion was stopped after overnight incubation and cleaned-up samples were vacuum dried then subjected to Phospho-enrichment (MagReSyn Zr-IMAC HP, ReSyn Biosciences). Finally, samples were re-dissolved with 10 min sonication in 0.15% N-Dodecyl-β-D-maltoside (DDM) in 0.1% Formic Acid.

LC-MS/MS analysis

Samples were analyzed by LC-MS/MS on a nanoElute 2 nano-HPLC (Bruker Daltonics) coupled with a timsTOF HT (Bruker Daltonics), concentrated over an Inertsil ODS-4 trap column (C18-coated particles, 3 cm), then bound to a monolithic capillary column (C18-coated polymer, 15 cm, Kyoto Monotech) heated at 50°C.

LC method: Solvent A: MS-grade H_2O + 0.1% formic acid; solvent B, 100% acetonitrile + 0.1% formic acid. The following gradients were used: total proteome samples, 60 min gradient, constant 0.30 nL/min flow, B percentage: 0 min = 5% / 35 min = 17% / 55 min = 35% / 60 min = 95%, followed immediately by a 5 min plateau at 95%; Phospho-Enriched Samples, 17.8 min gradient, constant 0.50 nL/min flow, B percentage: 0 min = 5%; 17.8 min = 30%, followed immediately by a 2 min plateau at 95%.

Total proteome samples were run using a Data-Independent Acquisition (DIA) method: M/Z range = 99.993933-1700 Th, ion mobility range = 0.7-1.4 1/K0; transfer time = 60 μs, pre-pulse storage time = 12 μs, enable high sensitivity modus = off, ion polarity = Positive, scan mode = dia-PASEF; TIMS parameters: ramp time = 180 ms, accumulation time = 180 ms; PASEF parameters: ms/ms scans = 4, total cycle time = 0 s, charge range = 0-5, intensity threshold for scheduling = 1500, scheduling target intensity = 15000, exclusion release time = 0.4 min, reconsider precursor switch = on, current/previous intensity ratio = 4, exclusion window mass width = 0.015 m/z, exclusion window v·s/cm^2 width = 0.015 V·s/cm^2. The DIA windows scheme: scan ranges: 34-1181/1181-1699/34-1134/1134-1699/34-1110/1110-1699/34-1063/1063-1699/34-1039/1039-1699/34-991/991-1699/34-944/944-1699/34-920/920-1699/34-873/873-1699/34-801/801-1699/34-754/754-1699/34-658/658-1699, isolation M/Z: 749.095/427.465/773.855/472.765/799.405/506.02/826.41/534.27/854.88/560.045/885.17/585.06/917.935/608.81/953.455/631.8/992.755/654.815/1036.99/677.845/1089.67/701.35/1159.37/725.11, isolation width: 24.45/54.5699999999999/25.0699999999999/36.03/26.03/30.48/27.98/26.02/28.96/25.53/31.6199999999999/24.5/33.9099999999999/23/37.1300000000001/22.98/41.47/23.0500000000002/47/23.01/58.3599999999997/24/81.04/23.52, collision energy: 42/28/42/28/42/29/43/29/43/29/43/30/44/30/44/30/44/31/45/31/45/32/46/32.

Phospho-enriched samples were run using a Data Dependent Method: M/Z range = 99.993933-1700 Th, ion mobility range = 0.7-1.4 1/K0; transfer time = 60 μs, pre-pulse storage time = 12 μs, enable high sensitivity modus = off, ion polarity = Positive, scan mode = MS/MS (PASEF); TIMS parameters: ramp time = 180 ms, accumulation time = 180 ms; PASEF parameters: ms/ms scans = 4, total cycle time = 0.93068 s, charge range = 0-5, intensity threshold for scheduling = 1500, scheduling target intensity = 15000, exclusion release time = 0.4 min, reconsider precursor switch = on, current/previous intensity ratio = 4, exclusion window mass width = 0.015 m/z, exclusion window v·s/cm^2 width = 0.015 V·s/cm^2.

Proteomics data analysis

Total proteome files were searched in DiaNN version 2.0.2 against an *in silico* predicted library. Phospho-enriched samples were searched in FragPipe version 22.0. Both searches were run with phosphorylation (STY) against the same *Arabidopsis thaliana* proteome from UniprotKB, with match-between-runs turned on. Results were filtered in both cases at 1% FDR.

The output PSM tables from both searches were converted to similar formats and combined, then re-processed using an in-house proteomics data analysis package, proteoCraft (pending publication). For consistent results, only phosphopeptide identifications from the search of phospho-enriched samples were retained, and conversely phospho-peptides were filtered out from the search of total proteome samples. Quantitative values from individual observations were re-normalized separately for phospho-enriched and total proteome samples, using the Levenberg-Marquardt procedure to minimize sample-to-sample differences. Peptide intensities were then corrected against the sample processing batch effect using sva::ComBat. Protein groups were inferred from observed peptides, and quantified using an in-house algorithm which: i) computes a mean protein-level profile across samples using individual, normalized peptidoform profiles (“relative quantitation” step), ii) following the best-flyer hypothesis, normalizes this profile to the mean intensity level of the most intense peptidoform (“unscaled absolute quantitation” step); for protein groups with at least 3 unique peptidoforms, only unique ones were used, otherwise razor peptidoforms were also included; Phospho-peptidoforms and their unmodified counterparts were excluded from the calculations. Estimated expression values were log10-converted and re-normalized using the Levenberg-Marquardt procedure, then tested for significance using a two-sided moderated t-test per samples group and a global F-test (limma). Significance thresholds were calculated using the Benjamini-Hochberg procedure for False Discovery Rate (FDR) values of 1%, 5%, 10 and 20%. For all tests, regulated protein groups were defined as those with a significant P-value and an absolute log2 ratio greater than 5% of intra-sample groups ratios. GO terms enrichment analysis was performed using topGO and ClueGO, comparing for each test regulated against observed protein groups. Statistical analysis was performed for Phospho-modified peptides as for protein groups, normalizing values to account for parent protein group(s) fold change.

Imaging via Confocal Laser Scanning Microscopy

For BFA treatment, seedlings were incubated in liquid AM+ medium supplemented with 50 μM BFA or together 10 μM NAA for 1 hr before washing with fresh AM+ medium for 30min. BFA bodies in whole *z*-stacks were analyzed using ImageJ. For colocalization evaluation, *pTOW::TOW-GFP* was co-immunostained with TGN, Golgi or ER markers. At least 12 individual roots were selected for each combination. Pearson correlation and Overlap coefficients were calculated using the Colocalization Finder plugin in ImageJ. For FRAP analysis of pPIN1:PIN1–GFP in endodermal cells, imaging was performed using a 40x objective with maximum scan speed to acquire 512 × 512 pixel images. Region of interest (ROI) with a 2 μm diameter was selected for bleaching using a 488 nm laser set to 100% power.

Fluorescence imaging was performed using a Zeiss LSM800 confocal laser-scanning microscope with the following excitation wavelength parameters: Cy3, 548 nm; Alexa Fluor 488, 488 nm.

Homology Analysis

The TOW protein sequence and its orthologous sequences were obtained from Phytozome 13 and aligned using ClustalW.[46] Neighbor-joining (NJ) phylogenetic analysis was conducted in MEGA 11[47] using protein Poisson distances and pairwise deletion of gap sites. Reliability of the phylogenetic tree was evaluated by performing 1000 bootstrap replicates. The consensus tree was visualized and annotated in iTOL v6 (https://itol.embl.de/).

External Data Sources

Arabidopsis gene and protein sequences are available from TAIR (https://www-arabidopsis-org.libraryproxy.ista.ac.at/). Sequences for *TOW* orthologous genes were obtained through a BLAST search with the AtTOW protein sequence in Phytozome 13 (https://phytozome-next.jgi.doe.gov/blast-search).

QUANTIFICATION AND STATISTICAL ANALYSIS

Statistical analyses were performed using GraphPad Prism 8 (GraphPad Software). One-way ANOVA followed by Tukey's multiple comparisons test was used for experiments involving a single factor. Two-way ANOVA followed by Tukey's multiple comparisons test was applied when two independent variables were analyzed. Statistical significance was determined at $P < 0.05$.